UNIVERSITY OF TURKU

Tank water-administered dabrafenib in BRAF-mutant zebrafish melanoma model

Institute of Biomedicine
MDP in Biomedical Sciences, Drug Discovery and Development
Master's thesis

Author:
Jenna Villman jmvill@utu.fi

Supervisors:
PhD, Doc. Ilkka Paatero; Turku Bioscience Centre, University of Turku and Åbo Akademi University
Academy Research Fellow, PhD, Doc. Kari Kurppa; Institute of Biomedicine, University of Turku

03.12.2025
Turku

Master's thesis

Subject: Institute of Biomedicine, MDP in Biomedical Sciences, Drug Discovery and Development
Author: Jenna Villman
Title: Tank water-administered dabrafenib in BRAF-mutant zebrafish melanoma model
Supervisors: PhD, Doc. Ilkka Paatero, Turku Bioscience Centre, University of Turku and Åbo Akademi University
Academy Research Fellow, PhD, Doc. Kari Kurppa; Institute of Biomedicine, University of Turku
Number of pages: 64 pages
Date: 03.12.2025

Melanoma is an aggressive skin cancer which incidence and mortality rates are increasing worldwide. The cancer often involves mutations in the *BRAF* gene, especially a V600E variant. Dabrafenib is a small-molecule BRAF inhibitor, which mechanism of action is based on the inhibition of mitogen-activated protein kinase (MAPK) signalling pathway. The aim of this study was to characterize the pharmacological properties of dabrafenib administered to the tank water using a zebrafish (*Danio rerio*) melanoma model.

Pharmacokinetics and pharmacodynamics were successfully assessed and described in healthy and BRAF V600E-mutated zebrafish and ZMEL1-GFP zebrafish melanoma cells. Mass spectrometry analysis of blood samples revealed that dabrafenib was absorbed and eliminated relatively fast. The drug and its metabolites were distributed into several abdominal organs which was seen in mass spectrometry imaging. During a two-week long treatment experiment, dabrafenib reduced tumour size significantly proving its efficacy in zebrafish. The changes after the drug administration could also be seen on a histological level with H&E staining. With immunohistochemistry and Western blotting, we were able to confirm dabrafenib's mechanism of action affecting extracellular signal-regulated kinase (ERK) phosphorylation of MAPK pathway. In addition, the drug had a dose-dependent effect on melanoma cell viability.

The need for translational models to study melanoma resistance, drug responses and therapies is increasing. Even though the BRAF V600E model has its limitations, this research provides a foundation to use tank-administered dabrafenib to study melanoma and melanoma therapies in zebrafish melanoma models. The study also supports the overall use of zebrafish as translational preclinical models.

Keywords: Dabrafenib, melanoma, zebrafish.

Table of contents

1 Introduction

1.1 Melanoma

The incidence and mortality rates of melanoma, aggressive skin cancer, are increasing worldwide (De Pinto et al., 2024). Melanoma is a malignant tumour originating from melanocytes, which are cells commonly found in the epidermis that synthesize melanin (Shain and Bastian, 2016). Melanocytes are mainly located in the skin, but also found in eyes, mucosa and other areas (Cichorek et al., 2013).

The characteristics of a melanoma lesions are described by ABCDE criteria: asymmetry, border irregularity, colour variation, diameter greater than 6 mm, and evolution (Abbasi et al., 2004). Melanoma is usually observed in the skin as cutaneous melanoma but can also develop in the eyes as uveal melanoma or in mucosal tissue as mucosal melanoma (Rabbie et al., 2019). Cutaneous melanoma can be classified into subtypes of which the superficially spreading melanoma is the most common (El Sharouni et al., 2020). Melanoma can spread to distant tissues, most usually to brain, liver, lungs, bones, and lymph nodes (Damsky et al., 2010).

1.1.1 Epidemiology

Melanoma accounts only for a fraction of skin cancers, but it is responsible for approximately half of skin cancer-related deaths. According to GLOBOCAN 2022 data, melanoma was the 17th most common cancer, while non-melanoma skin cancer (NMSC), including basal cell carcinoma and squamous cell carcinoma, is the 5th most common cancer (Ferlay et al., 2024). NMSC was 22th and melanoma 23th in the mortality statistics (Ferlay et al., 2024).

The incidence of melanoma has generally increased over time, but trends vary by region, with some areas showing stable rates in recent years (De Pinto et al., 2024). More than 330 000 new cases were diagnosed 2022 worldwide (Wang et al., 2025a). Highest incidence rates are in Oceania, North America and Northern and Western Europe (Wang et al., 2025a). The highest prevalence was shown in Europe followed by America (Wang et al., 2025a). The lowest incidence rates are found in Asia and Africa (Wang et al., 2025a). However, underreporting may contribute to these statistics (Cockburn et al., 2008). The melanoma incidence is estimated to increase 50% to 510 000 new cases by 2040 (Arnold et al., 2022).

Despite rising incidence, mortality rates have been declining in many world regions due to better awareness, screening, and advances in treatment (De Pinto et al., 2024). Approximately 59 000 deaths occur globally each year with the highest mortality rates being in New Zealand in 2022 (Wang et al.,

2025a). The melanoma mortality rates are estimated to increase 70% to 96 000 new deaths in 2040 (Arnold et al., 2022).

Age, sex and ethnicity have important demographic patterns. Melanoma can occur at any age, but the incidence rate increases in elderly (De Pinto et al., 2024; Wang et al., 2025a). Melanoma is one of the most common cancers in young adults (Miller et al., 2020). Men have higher overall incidence and mortality than women (Wang et al., 2025a). Fair-skinned individuals are at the highest risk while dark skinned individuals have lower incidence and higher mortality (Siegel et al., 2023).

1.1.2 Pathophysiology

Genetic risk factors and ultraviolet-induced damage play an important role in melanoma development from a benign nevus to malignant tumour (Carr et al., 2020). Ultraviolet A and B radiation induces DNA damage in melanocytes by forming cyclobutene pyrimidine dimers, which activate melanin production and generate reactive oxygen species, leading to oxidative damage in cells (Cadet and Douki, 2018). Several factors predispose to high ultraviolet radiation, including excessive sun exposure, sunburn in childhood, fair skin, multiple nevi and geographic location (Conforti and Zalaudek, 2021).

Several signal pathways have been connected to the pathogenesis of melanoma (Guo et al., 2021). As mitogen-activated protein kinase (MAPK) pathway, involving RAS, RAF, MEK and ERK proteins, regulates cellular proliferation and survival, mutations in this pathway are often driving tumorigenesis (Braicu et al., 2019). Hyperactivation of PI3K/AKT/mTOR pathway drives cell survival, metabolic reprogramming and therapy resistance (Jiang et al., 2025). Wnt/β-catenin pathway is important in cell proliferation, differentiation, migration and invasion in both homeostasis and cancer (Zhang and Wang, 2020). Other pathways are also found to be involved in melanoma initiation, progression, metastasis and modification of microenvironment including signal pathways linked to metabolism, inflammation and angiogenesis (Guo et al., 2021).

BRAF mutations are the most common genetic alteration in melanoma and predominantly observed in cutaneous subtypes (Lovly et al., 2012). In approximately 50 % of melanomas BRAF kinase mutations are present of which the substitution of valine at position 600 with glutamic acid (V600E) is the most common comprising 80% of these mutations (Davies et al., 2002; Lovly et al., 2012; Poynter et al., 2006). Other possible mutations include substitution of valine with lysine (V600K) or with aspartic acid (V600D) (Lovly et al., 2012). The mutations lock the BRAF serine-threonine-protein kinase to more active conformation, which leads to the phosphorylation of extracellular signal

regulated kinase (ERK) of MAPK pathway (Ascierto et al., 2012; Davies et al., 2002). *BRAF* mutation can occur as an early event in neoplastic transformation of melanocytes, but it alone is insufficient to induce malignant progression (Kumar et al., 2004; Pollock et al., 2003). Tumour suppressor *p53* is mutated in only 20% of melanomas (Hodis et al., 2012), but in most human melanomas the pathway function is disrupted by other genetic alternations, such as loss of *CDKN2A* (Berwick et al., 2006; Cilluffo et al., 2020).

In addition to *BRAF* mutations, several other key components of pathways implicated in melanoma are also frequently mutated. Mutations of *NRAS*, which are found in 25% of melanomas, activate the MAPK and PI3K/AKT/mTOR pathway by increasing the ratio of active to inactive RAS, which leads to constitutive downstream signalling through the PI3K and RAF (Hodis et al., 2012; Mendoza et al., 2011). NF1 loss is also connected to RAS hyperactivation (Nissan et al., 2014). *PTEN* and *MITF* mutations are often concurrent with *BRAF* and *NRAS* mutations (Garraway et al., 2005; Goel et al., 2006). *PTEN* mutations occur in 20% of melanomas (Goel et al., 2006). The loss of PTEN or AKT3 amplification causes PI3K/AKT pathway to active, which leads to cellular resistance to apoptosis (Jiang et al., 2025). Microphthalmia-associated transcription factor (MITF) is part of the Wnt/β-catenin pathway controlling the expression of genes involved in melanin production, cell cycle and apoptosis resistance (Hartman and Czyz, 2015). Approximately 15% of melanomas have *MITF* amplification (Cronin et al., 2009; Garraway et al., 2005).

Other mutations are more commonly found in other melanoma subtypes. *KIT* mutations are observed in approximately 22% of mucosal and 15% of acral melanomas, leading to constitutive activation of the receptor tyrosine kinase of MAPK pathway (Beadling et al., 2008). Mutations of *GNAQ* and *GNA11* are present in 45% and 35% of uveal melanomas, respectively (Van Raamsdonk et al., 2009; Van Raamsdonk et al., 2010). MAPK and AKT pathways and their most common mutations in melanoma are presented in Figure 1.

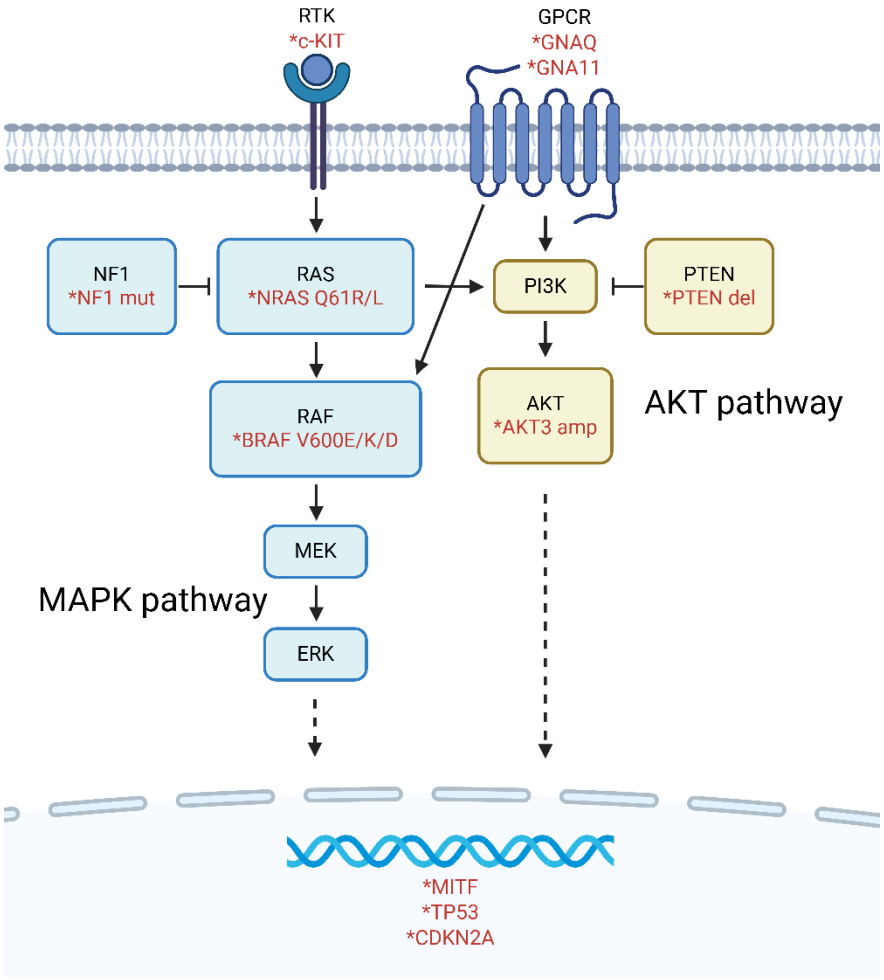

Figure 1. Mitogen-activated protein kinase (MAPK) and protein kinase B (AKT) pathway. Created with BioRender.com.

1.1.3 Treatment

Treatment options for melanoma include surgery, radiation, chemotherapy, immunotherapy and targeted therapy (Lopes et al., 2022; Natarelli et al., 2024). Primary treatment for early stage, thin and localized melanoma is surgical excision (Santamaria-Barria and Mammen, 2022). Sometimes lymph node dissection is also involved to assess the spread (Allard-Coutu et al., 2020; Santamaria-Barria and Mammen, 2022). Radiation therapy can be used after surgery to reduce recurrence, as an alternative when surgery is not possible, or to relieve symptoms caused by bone and brain metastases (Shi, 2015). Chemotherapy is nowadays rarely used to treat melanoma due to the limited effectiveness and high toxicity (Pham et al., 2023).

The newer treatment options include targeted therapies and immunotherapies (Lazaroff and Bolotin, 2023; Natarelli et al., 2024; Wang et al., 2025b). In targeted therapies, the aberrant and overactive signalling pathways are targeted directly by inhibiting the molecules responsible for tumour growth

and progression (Wang et al., 2025b). BRAF inhibitors, including dabrafenib, vemurafenib and encorafenib, are used for BRAF V600 mutated melanoma, where the MAPK pathway is overactive (Singh et al., 2023). In addition, the downstream of BRAF can be inhibited with MEK inhibitors, such as trametinib, cobimetinib and binimetinib, to prevent ERK activation (Ram et al., 2023). BRAF inhibitors are commonly associated with cutaneous toxicities, while MEK inhibitors cause gastrointestinal and ocular side effects (Ram et al., 2023; Singh et al., 2023). BRAF and MEK inhibitors are often used in combination therapies as they demonstrate greater efficacy used together (Dummer et al., 2018; Larkin et al., 2014; Long et al., 2014b). In addition to BRAF and MEK inhibitors, other targeted therapies can be considered off-label for patients with relevant mutations, such as imatinib for KIT amplification or mutation (Awada and Neyns, 2022). Targeted therapies and their inhibition of MAPK pathway is shown in Figure 2A.

Immunotherapies enhance patients' own immune system to fight melanoma (Wang et al., 2025b). Cytokine agonist interleukin-2 (IL-2) agonist aldesleukin boost immune system generally (Amaria et al., 2015). Immune checkpoint inhibitors (CPIs) target proteins on immune cells and helps the immune cells to attack the cancerous cells (Carlino et al., 2021). Ipilimumab blocks cytotoxic T-lymphocyte-associated antigen 4 (CTLA-4), which allows competitive CD28 bind to B7 on tumour cells more effectively, which increases T cell activity (Sobhani et al., 2021). Nivolumab and pembrolizumab blocks programmed cell death protein 1 (PD-1) on lymphocytes, and the ligand of PD-1 (PD-L1) on tumour cells can be blocked with atezolizumab (Javed et al., 2024). Normally the interaction between receptor and ligand transmits inhibitory signals to T cell, but blocking this interaction restores T cells cytotoxic function (Javed et al., 2024). Relatlimab binds to lymphocyte-activation gene 3 (LAG-3) and prevents it from binding to the inhibitory major histocompatibility complex II (MHC II) restoring the T cell activation and effector function (Andrews et al., 2022). Current CPIs and their binding sites are presented in Figure 2B.

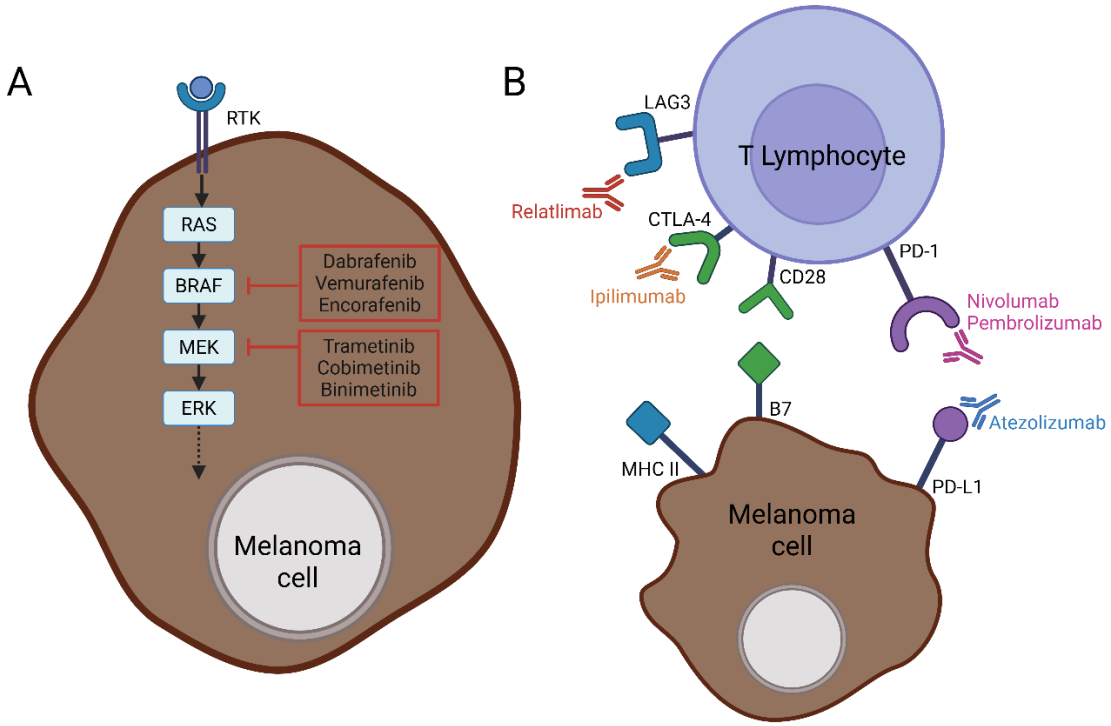

Figure 2. Current targeted therapies and immune checkpoint inhibitors in melanoma treatment. A. Mechanism of action of targeted drugs in MAPK signalling pathway. B. Sites of action of immune checkpoint inhibitors (CPIs). Adapted from Lazaroff and Bolotin, 2023. Created with BioRender.com.

In adoptive cell transfer patients' own T-lymphocytes are modified to amplify the tumour-targeting capability (Qian and Liu, 2025). Lifileucel is based on tumour-infiltrating lymphocytes that attack the melanoma cells (Sarnaik et al., 2021). Oncolytic virus therapies use viruses that infect and kill cancer cells while also alerting the immune system to attack them (Appleton et al., 2025). One example is intralesionally administered talimogene laherparepvec, also known as T-VEC, which is genetically modified herpes simplex virus (Ferrucci et al., 2021). There are also topical creams that stimulate local immune response, such as imiquimod (Vaienti et al., 2023). The adverse effect of immunotherapy is usually linked to autoimmunity affecting multiple organ systems (Kichloo et al., 2021).

The treatment of melanoma is challenging due to resistance development (Lazaroff and Bolotin, 2023; Lopes et al., 2022; Natarelli et al., 2024; Wang et al., 2025b). Melanoma adapts to its microenvironment through phenotype switching, metabolic and epigenetic reprogramming, and interactions with fibroblasts and immune cells (Hossain and Eccles, 2023). Secondary mutations can occur and alternative signalling pathways be activated (Czarnecka et al., 2020; Tangella et al., 2021). Tumours are also heterogeneous, which can harden their treatment (Ng et al., 2022). To overcome these challenges, combinations of several treatment modalities can be used together and new therapies

are being developed (Lazaroff and Bolotin, 2023; Lopes et al., 2022; Natarelli et al., 2024; Wang et al., 2025b).

The development of drugs for melanoma treatment is mainly focusing on targeted therapies and immunotherapy (Natarelli et al., 2024). Targeted therapy continues to expand beyond BRAF mutations, and for example tyrosine kinase inhibitor ripretinib for c-KIT mutated melanoma, pan-RAF inhibitor naporafenib for NRAS-mutated melanoma, and protein kinase C (PKC) inhibitor darovasertib for uveal melanoma are in clinical trials for melanoma treatment (De Braud et al., 2023; Janku et al., 2022; Piperno-Neumann et al., 2023). From preclinical studies, multiple new potential targets have been identified including chondroitin sulfate proteoglycan 4 (CSPG4) and melanotransferrin (CD228) (Chen et al., 2024; Zhang et al., 2024). In addition, DNA damage response inhibitors, including inhibitors of PARP, WEE1 and ATR, have demonstrated promising results in clinical trials (Maresca et al., 2022). In addition, melanoma neoantigen vaccines that encode patient-specific tumour antigens have gained interest (Blass et al., 2025; Gainor et al., 2024). Overall, the current pipeline reflects a shift toward more personalized strategies (Natarelli et al., 2024).

1.2 Dabrafenib

Dabrafenib (Tafinlar, GSK2118436) is a potent, selective and reversible rapidly accelerated fibrosarcoma (RAF) kinase inhibitor, especially to the constitutionally active mutant serine-threonine kinase BRAF (King et al., 2013). This small-molecule drug is approved as a single agent for BRAF V600E-mutated unresectable or metastatic melanoma by European Medicines Agency (EMA) and U.S. Food & Drug Administration (FDA) (European Medicines Agency, 2013; U.S. Food & Drug Administration, 2013). It has been approved as a combination therapy with MEK inhibitor trametinib for BRAF V600E and BRAF V600K -mutated melanoma and BRAF V600E-mutated non-small cell lung cancer and anaplastic thyroid cancer (European Medicines Agency, 2013; U.S. Food & Drug Administration, 2013; Spain et al., 2016).

1.2.1 Effectiveness

Dabrafenib's clinical efficacy is evaluated as a monotherapy and in a combination. During the phase III BREAK-3 trial, dabrafenib as a monotherapy increased the overall survival (OS) and progression-free survival (PFS) compared to chemo drug dacarbazine (DTIC) in patients with unresectable stage 3 BRAF V600E-mutated cancer. Median OS was 15.6 months for DTIC and 20.0 months for dabrafenib group, while the median PFS was increased 2.5-fold from 2.9 to 6.7 months (hazard ratio, HR=0.35) (Hauschild et al., 2012). From five-year analysis OS and PFS were found to be 24% and

12% for dabrafenib and 22% and 0% for DTIC group (Hauschild et al., 2020). During the trial the objective response rate (ORR) was 50%, while 3% of the patient had a complete response (CR) and 47% partial response (PR) (Hauschild et al., 2012). The median time to response (TTR) was 6.3 weeks and the estimated median duration of response (DoR) was 5.5 months (Hauschild et al., 2012). Dabrafenib is also efficient on BRAF V600E-mutated brain metastases with response rate being 39% with no prior local treatment and 31% with prior treatment (Long et al., 2012).

The combination of dabrafenib and trametinib enhanced the results compared to only dabrafenib for BRAF V600E or BRAF V600K mutated melanoma in COMBI-D trial. Dabrafenib in combination with trametinib has further improved the PFS from 8.8 to 11.0 months (HR=0.67) (Long et al., 2015). The OS rate for only-dabrafenib and for combination groups were, respectively, 85% and 93% at 6-month timepoint and 42% and 51% at 2-year timepoint (Long et al., 2014b; Long et al., 2015). Combined results from COMBI-V and COMBI-D trials demonstrated that PFS and OS were 19% and 34% for the combination group at five years (Robert et al., 2019). In patients with BRAF V600E mutation treated with dabrafenib and trametinib ORR was 68%, CR 11% and PR 57%, and the corresponding values for dabrafenib-only group were 53%, 9% and 44% (Long et al., 2014b). The median DoR was 12.9 months in combination treatment group and 10.6 months in dabrafenib-only group (Long et al., 2015).

1.2.2 Mechanism of action

Dabrafenib targets especially the V600E mutated BRAF proteins of MAPK pathway and downregulates its downstream signalling by decreasing MEK and ERK phosphorylation, which leads to cell cycle arrest, inhibits melanoma cell proliferation and results in cell death (King et al., 2013). In combination treatment with trametinib, MEK is also directly inhibited for more effective blocking (King et al., 2013). MAPK pathway inhibition was not reported in wild-type cells after dabrafenib treatment possible due to the paradoxical induction of MAPK pathway through CRAF downstream signalling (Carnahan et al., 2010; Hatzivassiliou et al., 2010; Heidorn et al., 2010). Dabrafenib has also a possible effect on immune modulation as mutated BRAF kinase inhibition leads to decreased production of immunosuppressive cytokines, which improves the anti-tumour activity (Ilieva et al., 2014).

1.2.3 Pharmacological properties

Dabrafenib's pharmacokinetics and -dynamics are well-known in humans. The recommended dose of dabrafenib is 150 mg orally two times a day under faster conditions (Falchook et al., 2014).

Absolute oral bioavailability of a single dose of 150 mg is 95% (Denton et al., 2013), so it is absorbed almost completely. Its absorption time from the gastrointestinal tract to maximum serum concentration of 2160 ng/ml is 2.0 h (Falchook et al., 2014). Following repeated administration, dabrafenib exposure decreases over time (Falchook et al., 2014). Age, sex and body weight has no clinically significant influence on plasma exposure (Oullet et al., 2014). Dabrafenib is substrate of P-glycoprotein (P-gp) and breast cancer resistance protein (BCRP), which limits its penetration across the blood-brain barrier (Mittapalli et al., 2013).

Dabrafenib is metabolized mainly by CYP3A4 and CYP2C8 (cytochrome P450) enzymes to form hydroxy-dabrafenib, which is further oxidised to carboxy-dabrafenib and can still be non-enzymatically decarboxylated in the gut to desmethyl-dabrafenib as shown in Figure 3 (Bershas et al., 2013). Desmethyl-dabrafenib is further processed by CYP3A4 into oxidative metabolites (Bershas et al., 2013). Carboxy- and desmethyl-dabrafenib accumulate after repeated dosing, and hydroxy-dabrafenib contributes likely to the pharmacological activity (Bershas et al., 2013). Approximately 70% of the drug is excreted to faeces, mostly as an unchanged drug, but urinary excretion was accounted for some of the metabolites (Bershas et al., 2013).

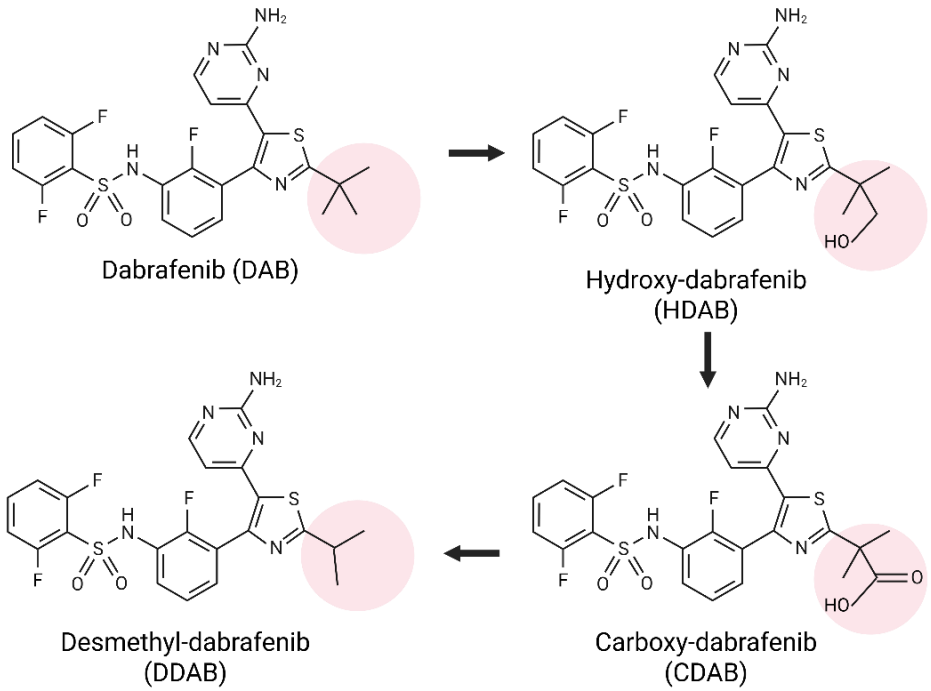

Figure 3. Dabrafenib and its main metabolites. Adapted from Puszkiel et al., 2019. Created with BioRender.com.

Elimination half-life and plasma clearance are 2.6 h and 12.0 L/h after intravenous administration and 4.8 h and 14.0 L/h after a single oral dose (Denton et al., 2013). The longer half-life after oral administration is probably a result of prolonged absorption that limits the elimination rate, which is also called 'flip-flop pharmacokinetics' (Denton et al., 2013). A time-dependent increase in clearance is observed with multiple dosing suggesting autoinduction of metabolism via CYP3A4 (Falchook et al., 2014). The phenomenon causes the steady state to be reached after 14 days of bid dosing (Ouellet et al., 2014).

1.2.4 Limitations

As with all therapies, dabrafenib has its own limitations including broad spectrum of response, adverse effects and resistance. The spectrum of response to dabrafenib therapy is broad as response depth and duration are heterogeneous. Roughly half of patients with BRAF V600E mutant metastatic melanoma have objective responses with dabrafenib-treatment (Hauschild et al., 2012; Long et al., 2014b). Responses to the treatment can be rapid but are often short-lived even though some patients have durable long-term control (Hauschild et al., 2012; Long et al., 2015).

Side effects with dabrafenib are common but often manageable. The most common adverse effects of dabrafenib include hyperkeratosis, headache, fever, fatigue, arthralgia and alopecia (Hauschild et al., 2012; Long et al., 2014b). COMBI-D trial demonstrated that adverse events occurred in 87% of patients in dabrafenib-only group and in 90% of patients in dabrafenib-trametinib combination group. Compared to dabrafenib-only group, the patients treated with the combination had fewer cases of cutaneous events, alopecia, and hand-foot syndrome while pyrexia was more common in the combination treatment group (Long et al., 2015). Among patients receiving dabrafenib monotherapy, 13% required a dose reduction and 5% discontinued treatment permanently, compared with 25% and 9%, respectively, in the combination therapy group (Long et al., 2015).

The dabrafenib treatment efficacy differences between patients due to broad range of molecular mechanisms (Hauschild et al., 2012; Zhong et al., 2022). The most common resistance mechanism is reactivation of MAPK pathway through BRAF amplification, alternative splicing of BRAF, overexpression of RTKs, activating mutations of CRAF, NRAS and MEK and loss of NF1 (Zhong et al., 2022). Activating mutations in other proliferative pathways, such as PI3K/AKT/mTOR, can also be behind resistance (Zhong et al., 2022). Combination treatment strategies improve response rates and partially overcome resistance: Combination of BRAF inhibitor dabrafenib and MEK inhibitor trametinib delays MAPK pathway reactivation (Long et al., 2014a). Addition of a PI3K/AKT/mTOR

inhibitors or next-generation RAF inhibitors to dabrafenib treatment target the bypass pathways and are currently under investigation (Wang et al., 2021; Yaeger et al., 2024).

1.3 Zebrafish

Zebrafish (*Danio rerio*) is a well-established vertebrate model whose use in biomedical research continues to expand (Teame et al., 2019). The similarity between human and zebrafish genomes and physiology, small size and low maintenance makes zebrafish a good tool to model diseases (Hason and Bartůněk, 2019; Patton et al., 2021). Considering melanoma, the zebrafish model not only provides insights into the fundamental mechanisms of tumour initiation, progression and metastasis but also serves as a valuable system for identifying and evaluating novel therapeutic agents (Frantz and Ceol, 2020). Both transgenic and transplantation models have been established (Frantz and Ceol, 2020; Hason and Bartůněk, 2019; Van Rooijen et al., 2017).

1.3.1 Advantages and challenges

The zebrafish offers multiple advantages as an experimental model. The small size makes zebrafish an easy and affordable model organism to maintain (Aleström et al., 2020). The short reproduction interval and large number of embryos guarantee efficient breeding in laboratory conditions all year round (Nasiadka and Clark, 2012). Fertilization occurs externally after which rapid embryonic development inside transparent chorion begins (Kimmel et al., 1995). There are also genetically transparent adult strains, such as casper (White et al., 2008). These characteristics enables the effective use of zebrafish in large-scale drug screenings (Patton et al., 2021).

Human and zebrafish genomes have a high level of similarity with estimated 70% of orthologous genes, and approximately 80% of known human disease genes have orthologues in zebrafish (Howe et al., 2013). This also means that the cell signalling pathways are mainly conserved including MAPK pathway important for melanoma progression (Krens et al., 2006). However, the teleost genome is duplicated and involves genes in more than one copy (Howe et al., 2013). The genes can be easily modified to create mutated or transgenic disease models (Frantz and Ceol, 2020; Hason and Bartůněk, 2019; van Roojen et al., 2017).

Even though zebrafish share many physiological similarities to humans, there are also notable differences. Considering the skin structure, fish have epidermis, dermis and hypodermis similarly to mammals (Hawkes, 1974). While the human epidermis is stratified and keratinized, the fish epidermis consists of a few layers of living cells covered in mucus (Henrikson and Matoltsy, 1967). In addition,

they possess scales located in dermis (Hawkes, 1974). Zebrafish also have three pigment cell types: dark melanophores, yellow xanthophores and reflective iridophores (Kelsh et al., 1996). Melanophores synthesize melanin and are considered functional equivalents to human melanocytes (Camp and Lardelli, 2001). Zebrafish pigment cells are found in hypodermis while human melanophores are located in epidermis (Cichorek et al., 2013; Hirata et al., 2003).

Pathogenesis of diseases is also mainly conserved. Melanoma of humans and zebrafish have many molecular and physiological similarities including the presence of specific gene mutations, initiation from melanocytes and ability to metastasise (Frantz and Ceol, 2020). There are still some differences in, for example, immune responses and tumour microenvironment (Frantz and Ceol, 2020). Similarly to humans, zebrafish with BRAF V600E mutation alone developed only nevi, and additional loss-of-function mutation of tumour suppressor gene *tp53* was required for the tumour progression (Patton et al., 2005).

The differences have also an effect on drug studies. Administering drugs via conventional routes, such as orally or intravenously, is technically challenging, whereas administration directly in the water is simple but does not mimic human administration and results in unknown internal drug concentration (MacRae and Peterson, 2023). Drug metabolism pathways differ as zebrafish have many CYP families, but some of them differ in substrate specificity and expression (Goldstone et al., 2010). For example, zebrafish Cyp3a65 is similar to human CYP3A4 but not identical in activity (Goldstone et al., 2010). Zebrafish are poikilothermic fish with optimal living temperature of 28°C, which is lower than human temperature and can affect multiple aspects, such as tumour growth and drug response (Hason and Bartůněk, 2019). Blood-brain barrier in zebrafish is functionally similar but structurally less complex, which leads to differences in drug penetration to central nervous system (Quiñonez-Silvero et al., 2020). Limited pharmacological data in zebrafish makes human dose translation challenging and can lead to misleading conclusions about drug toxicity and efficacy (MacRae and Peterson, 2023).

1.3.2 Genetic models

Zebrafish have been genetically modified to develop melanoma to study cancer biology and treatments (Frantz and Ceol, 2020; Hason and Bartůněk, 2019; Van Rooijen et al., 2017). Both stable genetic modifications, such as transgenes or mutations, and transient manipulations, including gene overexpression or downregulation, can be achieved (Li et al., 2021). The conventional models are generated by injecting nucleic acids into one-cell stage embryos (Li et al., 2021).

Multiple gene-editing techniques have been established in zebrafish including Tol2 transposon based transgenesis and clustered regularly interspaced short palindromic repeats (CRISPR) system (Li et al., 2021). In Tol2 transposon based transgenesis, a DNA construct flanked by Tol2 recognition sites is injected with Tol2 transposase mRNA into embryos and the transposase integrates the construct into the genome (Kawakami et al., 2000). There are several systems utilizing this transgenesis, such as MiniCoopR (Ceol et al., 2011). CRISPR/Cas9 method is based on CRISPR sequences that are complementary with certain DNA sequence and guide Cas9 enzyme to the targeted area, which then removes or pastes the wanted DNA sequence to the genome (Ablain et al., 2015).

Zebrafish with loss of *mitfa* lacks melanocytes (Lister et al., 1999). When MiniCoopR vector that has a mitfa promoter and *BRAF* ^{V600E} gene is injected in the *mitfa* (-/-) and *p53* (+/-) embryos, the melanocytes are mosaically rescued and express the mutated *BRAF* gene leading to tumour development (Patton et al., 2005). Using this system, the study found several amplified genes in human melanoma, including *SETDB1*, to cooperate with *BRAF* V600E to enhance melanomagenesis (Ceol et al., 2011). Also, antirheumatic drug leflunomide was found to inhibit strongly melanoma initiation and progression in a drug screening using this model (White et al., 2011).

Similarly, other mutations typical to human cutaneous melanoma, such as mutations of HRAS and NRAS, have been modelled in zebrafish (Dovey et al., 2009; Santoriello et al., 2010). Antifungal clotrimazole was identified in drug repurposing screening using HRAS^{G12V} mutated zebrafish model to reduce melanoma tumour growth and invasion (Precazzini et al., 2020). In addition, zebrafish models with GNAQ and GNA11 mutations have developed uveal melanoma similar to humans (Mouti et al., 2016; Thomas et al., 2016). Compared with sun-exposed human melanomas, zebrafish melanomas exhibit fewer mutations and less genetic heterogeneity, as human tumours retain UV-induced mutations over time (Yen et al., 2013).

1.3.3 Transplantation models

Melanoma tumour pathogenesis, invasiveness and therapies can be studied through tumour cell transplantation (Frantz and Ceol, 2020; Hason and Bartůněk, 2019; Van Rooijen et al., 2017). The transparency of zebrafish embryos and transparent adult fish strains make the cancer cell proliferation easy to follow (White et al., 2008). Tumour cells can be transplanted into zebrafish as allografts, when transferred between individuals of the same species, or as xenografts, when transferred between individuals of different species (Hason and Bartůněk, 2019). The transplantation is typically performed into intraperitoneal cavity of adult zebrafish or into cardinal vein or yolk sac of embryos 48 hpf (Hason and Bartůněk, 2019).

Transplant rejection is not an issue during the first weeks of zebrafish life as the adaptive immune system onsets at 7 days post fertilization (dpf), and the cells responsible for immune competence mature until 4 weeks post fertilization (Lam et al., 2004; Langenau et al., 2004). In adult zebrafish, rejection can be avoided by sub-lethal irradiation to deplete immune cells (Traver et al., 2004) or use immunodeficient fish (Moore et al., 2016; Tang et al., 2014; Yan et al., 2019).

Melanoma allografts have been generated with both primary cancer cells and established cancer cell lines. ZMEL1 cell line originates from melanomas of transgenic zebrafish lacking *mitfa* and *tp53* and expressing BRAF V600E is widely used to study melanoma pathogenesis, metastasis, microenvironment and inhibition (Heillman et al., 2015). Studies using ZMEL1 melanoma allografts have showed, for example, that tumour-derived extracellular vesicles can activate macrophages and promote metastasis (Hyenne et al., 2019), and that signals from microenvironment induce phenotype switching after metastatic dissemination (Kim et al., 2017).

Human melanoma has been widely studied in zebrafish through xenografts (Hason and Bartůněk, 2019). Early studies demonstrated that human melanoma cells injected into zebrafish embryos proliferate, migrate and induce angiogenesis (Haldi et al., 2006; Lee et al., 2005). Invasive melanoma cells co-invade with poorly invasive cells to maintain tumour heterogeneity (Chapman et al., 2014). Melanoma xenografts were found to secrete embryonic morphogen Nodal and antiapoptotic bcl-xL which promote melanoma aggressiveness (Gabellini et al., 2018; Topczewska et al., 2006). Tumour-derived metabolites, such as lactate, influence immune cell behaviour and angiogenesis (Yin et al., 2024). In addition, tumour innervation and neurotransmitter signalling can shape melanoma cell migration and tumour progression (Lorenzini et al., 2025).

Zebrafish patient-derived xenograft (zPDX) models are an emergencing tool to study human tumour behaviour and therapeutic response (Chen et al., 2021; Sugino et al., 2025). In the future, so called avatar models could be established to investigate efficacy and resistance of multiple drugs before choosing a treatment for a patient (Sugino et al., 2025). zPDX platform has been established for uveal melanoma by implanting uveal melanoma spheroids into zebrafish embryos (Yin et al., 2023). The model recapitulated the molecular features, invasive behaviour and drug responsiveness of the parental tumour (Yin et al., 2023). However, these models require further investigation for them to be useful in personalized medicine (Chen et al., 2021; Sugino et al., 2025).

1.4 Aim of the study

Our goal was to demonstrate that administering dabrafenib via tank water is a feasible approach for treating BRAF V600E mutant melanoma in zebrafish. Only vemurafenib of BRAF inhibitors has been tested in adult zebrafish by oral gavage and pellets, which are challenging and unreliable administration routes due to technical administration or uneven dosing (Dang et al., 2016; Lu and Patton, 2022). We sought to show that direct drug administration into tank water is a practical and efficient delivery method for long-term treatment.

Understanding pharmacokinetics of small molecule inhibitors in zebrafish is limited. We investigated both pharmacokinetics and pharmacodynamics of dabrafenib in BRAF V600E mutant zebrafish and zebrafish melanoma cells. We hypothesized that the key parameters, including absorption, elimination, distribution and dose-response would resemble those observed in humans. We aimed to demonstrate that tank water-administered dabrafenib is an effective treatment for melanoma in zebrafish and to confirm its known mechanism of action, inhibition of the downstream MAPK signalling pathway, in this model.

In addition, our objective was to show that commonly used BRAF V600E mutant melanoma zebrafish serves as a robust model for studying dabrafenib and other small molecule melanoma therapies (Frantz and Ceol, 2020; Van Rooijen et al., 2017). We further hoped that these findings will strengthen the rationale for using zebrafish as a preclinical model for drug research in melanoma and other cancers.

1.5 Summary

Melanoma is a skin cancer that appears in cutaneous, uveal and mucosal tissues (Rabbie et al., 2019). Excessive ultraviolet light and certain genetic mutations are major risk factors in its development (Carr et al., 2020). The most common mutation is BRAF V600E (Lovly et al., 2012). The burden of melanoma is increasing globally making it an interesting and important research topic and drug development target (De Pinto et al., 2024). Nowadays, the most commonly used melanoma therapies are immunotherapies and targeted therapies, including dabrafenib (Wang et al., 2025b).

Dabrafenib is a small molecule BRAF inhibitor approved by both EMA and FDA for the treatment of melanoma (European Medicines Agency, 2013; U.S. Food & Drug Administration, 2013). Its pharmacokinetics and pharmacodynamics are well-known in humans (Falchook et al., 2014). As with all melanoma therapies, the tumours can develop resistance to dabrafenib (Zhong et al., 2022). To

overcome this challenge, more studies are needed to be conducted considering resistance and development of new therapies.

Zebrafish models are more commonly used in biomedical research including melanoma studies due to its advantages as a small vertebrate with high reproductivity and its similarity in genetics and physiology to humans (Hason and Bartůněk, 2019). Both genetic and transplantation zebrafish models have been established of which BRAF V600E-mutated is one of the most commonly used (Frantz and Ceol, 2020). However, it is important to remember that no animal model human diseases perfectly.

The aim of this study was to assess the feasibility and translatability of BRAF V600E-mutated zebrafish model treated with tank water-administered dabrafenib. As pharmacological understanding of small molecule inhibitors in zebrafish is limited, we studied dabrafenib's pharmacokinetics and efficacy. BRAF inhibitors have been previously administered orally, but direct administration into tank water has not been demonstrated. We wanted to test if zebrafish models are useful for melanoma and other cancer drug studies.

2 Results

2.1 Establishment of zebrafish melanoma model

A BRAF V600E-mutated zebrafish melanoma model was successfully established by injecting plasmid DNA containing the mutated region into 1dpf embryos using Tol2 transposon system. Approximately 2% of the injected embryos developed individual dark cells and patches of pigment suggesting incipient neoplasia at 3days post injection (dpi, data not shown). However, all embryonic tumours did not develop into melanomas in adult fish. The size, location and number of tumours varied among fish. Pigmented areas could cover large surfaces or appear as discrete clusters in skin, fins and eyes (Figure 4). Yellowish xanthophore tumours were also observable in some fish.

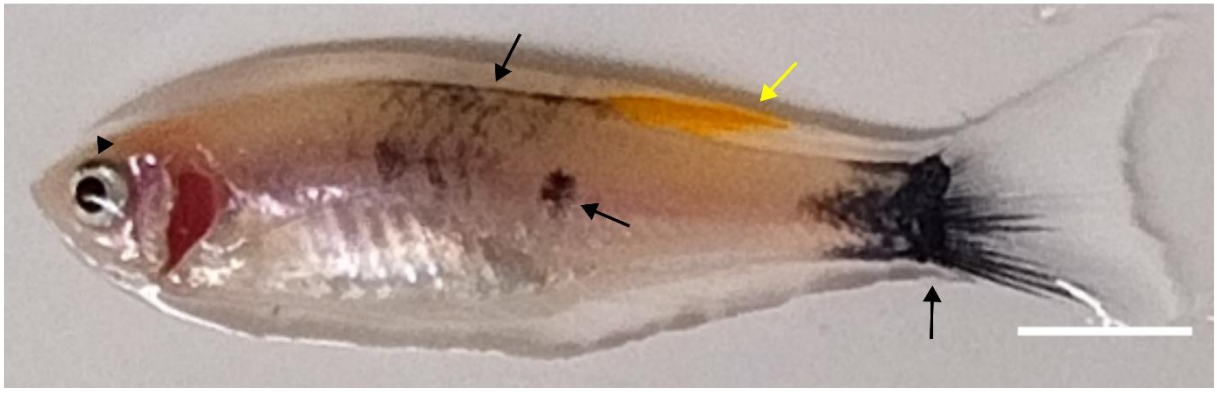

Figure 4. Zebrafish melanoma model. Black arrows point to cutaneous melanoma, black arrow head to uveal melanoma and yellow arrow to xanthophore tumour. Scale bar = 5 mm.

2.2 Pharmacokinetics of dabrafenib in zebrafish

2.2.1 Absorption and elimination

Dabrafenib's absorption and elimination were studied in zebrafish melanoma model by administrating the inhibitor in the tank water. Dabrafenib concentrations were measured by mass spectrometry from blood samples taken in several timepoints after starting and discontinuing dosing (n=2-4 fish per timepoint). The collected blood sample volume varied between 0.6-6.4 µl.

Effective dabrafenib concentration (IC50=0.19 µM, according to 2.3.1 Cell viability) was exceeded already at the first 0.5-hour timepoint after 10 mM administration into the tank water. The highest dabrafenib concentration (c_{max}), 13.7µM (SD 6.6), was reached at 4-hour time point (t_{max}). Dabrafenib concentration after 24-hour administration was 2.7 µM (SD 2.3) and after 2-week administration 5.9

µM (SD 3.3). The parameters of dabrafenib's primary metabolite, hydroxy-dabrafenib, aligned with dabrafenib's pharmacokinetic properties. Corresponding values for hydroxy-dabrafenib, were 0.64 µM (SD 0.061), 0.15 µM (SD 0.19) and 0.14 µM (SD 0.12).

We were unable to fit a representative curve for absorption. The fitted curve for elimination over time showed good fit for dabrafenib (weighted R^2 0.95) and hydroxy-dabrafenib (weighted R^2 0.81). During dabrafenib dosing, the concentration increased over the first 4 hours before gradually declining (Figure 5A). After discontinuing dosing, the concentration declined steadily (Figure 5B). Similar trends could be seen for hydroxy-dabrafenib (Figures 5C and 5D). Half-life ($t_{1/2}$) of dabrafenib elimination was 1.0 h (95% CI 0.8-1.4), and that of hydroxy-dabrafenib was 1.6 h (95% CI 0.6-8.1).

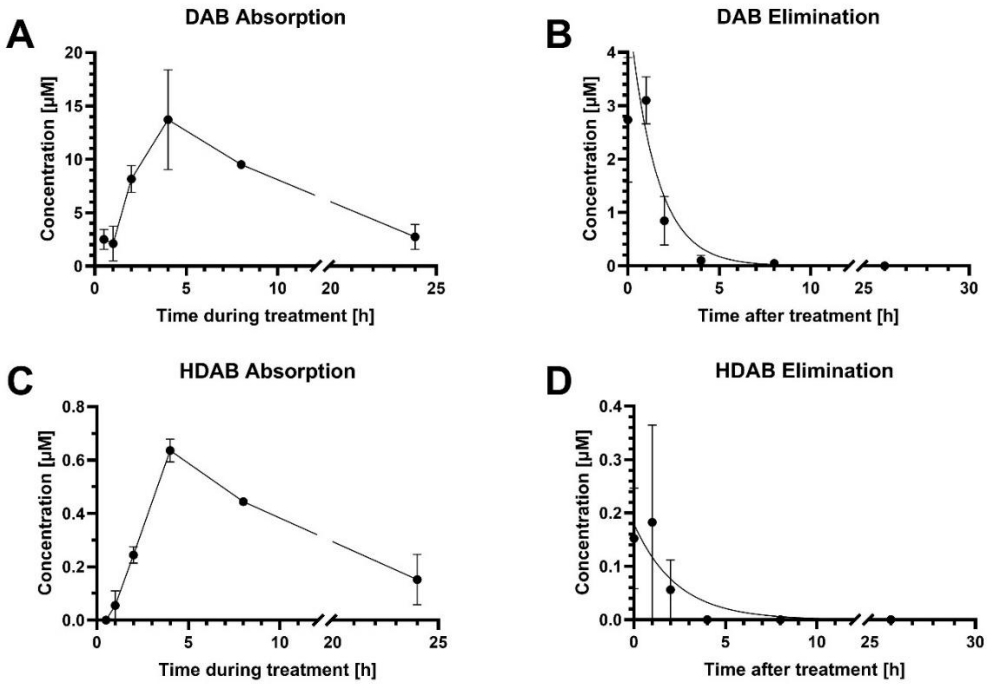

Figure 5. Absorption and elimination of dabrafenib and hydroxy-dabrafenib with dabrafenib. Concentrations were measured from blood samples taken at multiple time points following 10 mM dabrafenib administration to the tank water and discontinuing it using LC-MS. A. Absorption curve of dabrafenib (DAB). B. Elimination curve of dabrafenib (DAB). C. Absorption curve of hydroxy-dabrafenib (HDAB). D. Elimination curve of hydroxy-dabrafenib (HDAB). The mean and SEM are presented for each time point (n = 2-4 fish / time point). Note the discontinuity in the X-axes and differences between Y-axes.

2.2.2 Distribution

We observed dabrafenib, and its hydroxy- and desmethyl-metabolites in zebrafish, but we were unable to detect any carboxy-dabrafenib using mass spectrometry imaging (Figure 6, Supplementary Figure 1). Dabrafenib could be observed in many abdominal organs and gills (Figure 6A). Hydroxy-dabrafenib and desmethyl-dabrafenib were mainly seen in the gut (Figure 6B and 6D), but in other

abdominal tissues as well. We did not observe dabrafenib or its metabolites in brain or skeletal muscle. We could not identify the tissues more precisely in H&E staining due to the brokenness of the samples (Figure 6E).

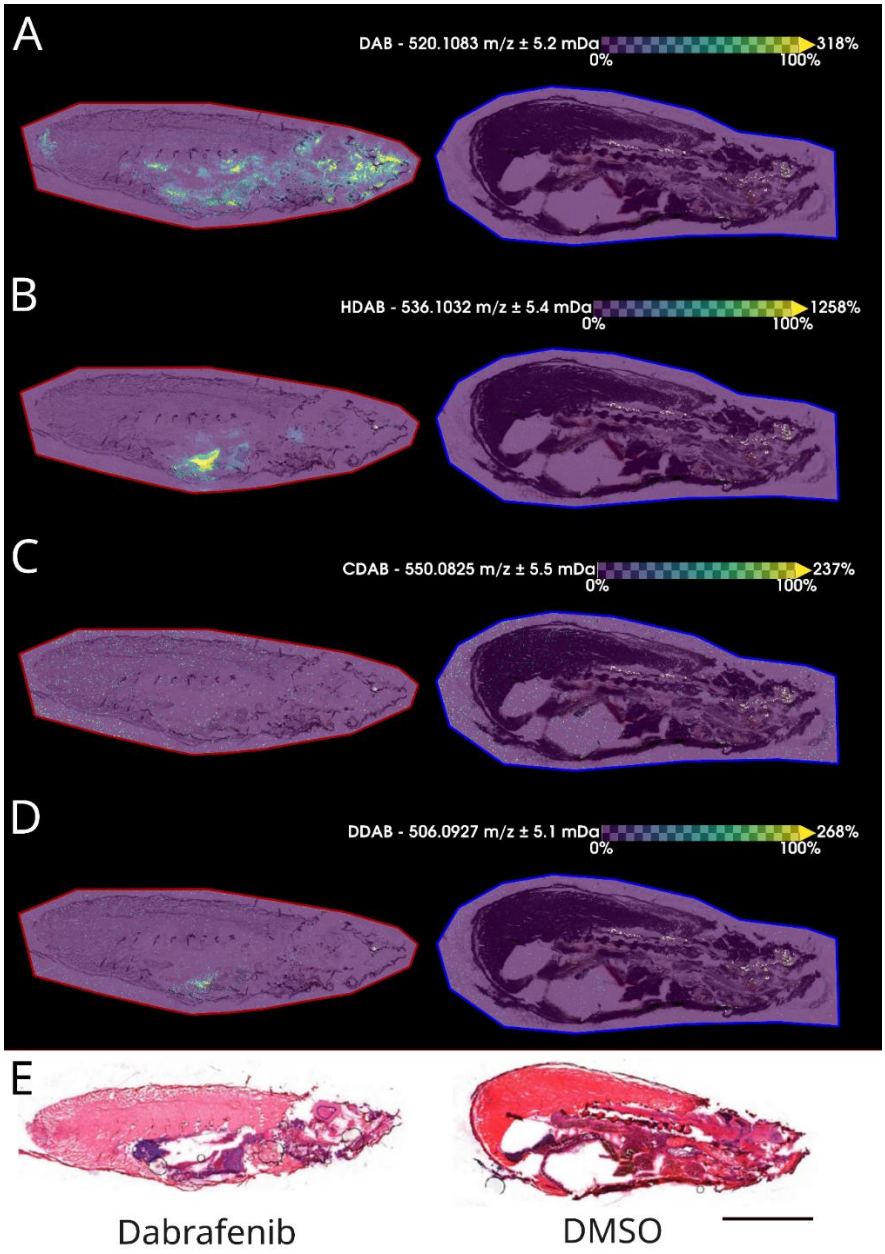

Figure 6. Localization of dabrafenib and its metabolites. Mass spectrometry imaging was performed using MALDI-MSI to visualise spatial distribution of dabrafenib and its most important metabolites in dabrafenib-treated (n=6) and control (n=2) zebrafish. On left is a dabrafenib-treated fish (red annotation) and on right a control fish (blue annotation). Colour maps indicate relative abundance. A. Dabrafenib (DAB). B. Hydroxy-dabrafenib (HDAB). C. Carboxy-dabrafenib (CDAB). D. Desmethyl-dabrafenib (DDAB). E. Hematoxylin-eosin staining. Scale bar = 5 mm.

2.3 Phamacodynamics of dabrafenib in zebrafish

2.3.1 Dose-response

Efficacy of dabrafenib in zebrafish melanoma model was verified in zebrafish melanoma cell line, ZMEL1-GFP, using CellTiter-Glo assay. Dose-dependent decrease was observed in cell viability with increasing dabrafenib concentrations (Figure 7). The IC50 value was 190 nM (95% CI 150-240 nM). The fitted curve of dose-response showed a good fit (R^2 0.80).

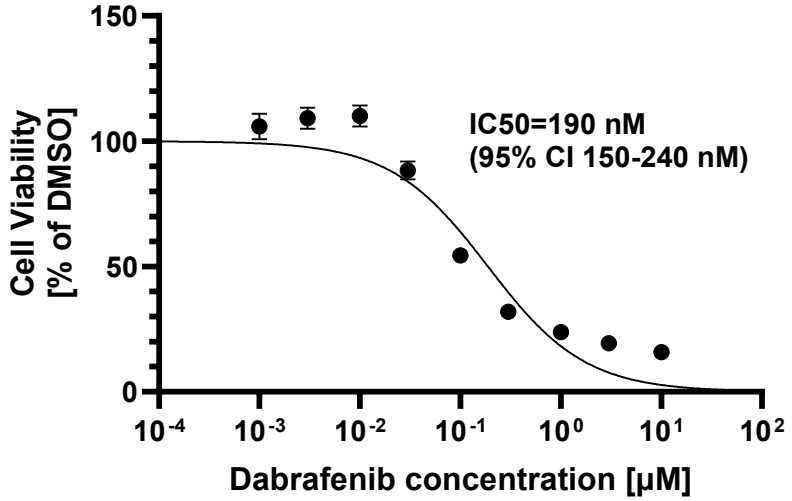

Figure 7. Cell viability with increasing dabrafenib concentrations. ZMEL1-GFP cells were treated with increasing concentrations of dabrafenib (from 1 nM to 10 mM) for 72 hours, and viability was assessed using CellTiter-Glo assay. The cell viability is expressed as the percentage of living cells compared to the control cells with 0 µM dabrafenib. The mean and SEM of four replicate studies are presented.

2.3.2 Efficacy

Zebrafish with visible melanoma tumours were treated for 2 weeks with dabrafenib to observe drug response. There was obvious visual difference between dabrafenib-treated and control fish with cutaneous melanoma: the tumour lightened and the area decreased (Figure 8A). The change in tumour size was between -98.3% and +26.1% for dabrafenib treated fish and between -41.9% and +30.7% for control fish (Figure 8B). The mean change for dabrafenib treated fish was -55.5% (SD 50.1, n=12) and for control fish +0.32% (SD 24.8, n=11) (Figure 8C). The difference was statistically significant (p=0.0032).

There seemed to be non-responder and responder group in the dabrafenib-treated fish, while the control values are around the baseline (Figure 8D). Response rate was 67% (n=8/12). The size of the

tumours that responded to dabrafenib treatment decreased during the two-week experiment while control and non-responder groups stayed approximately the same size (Figure 8E).

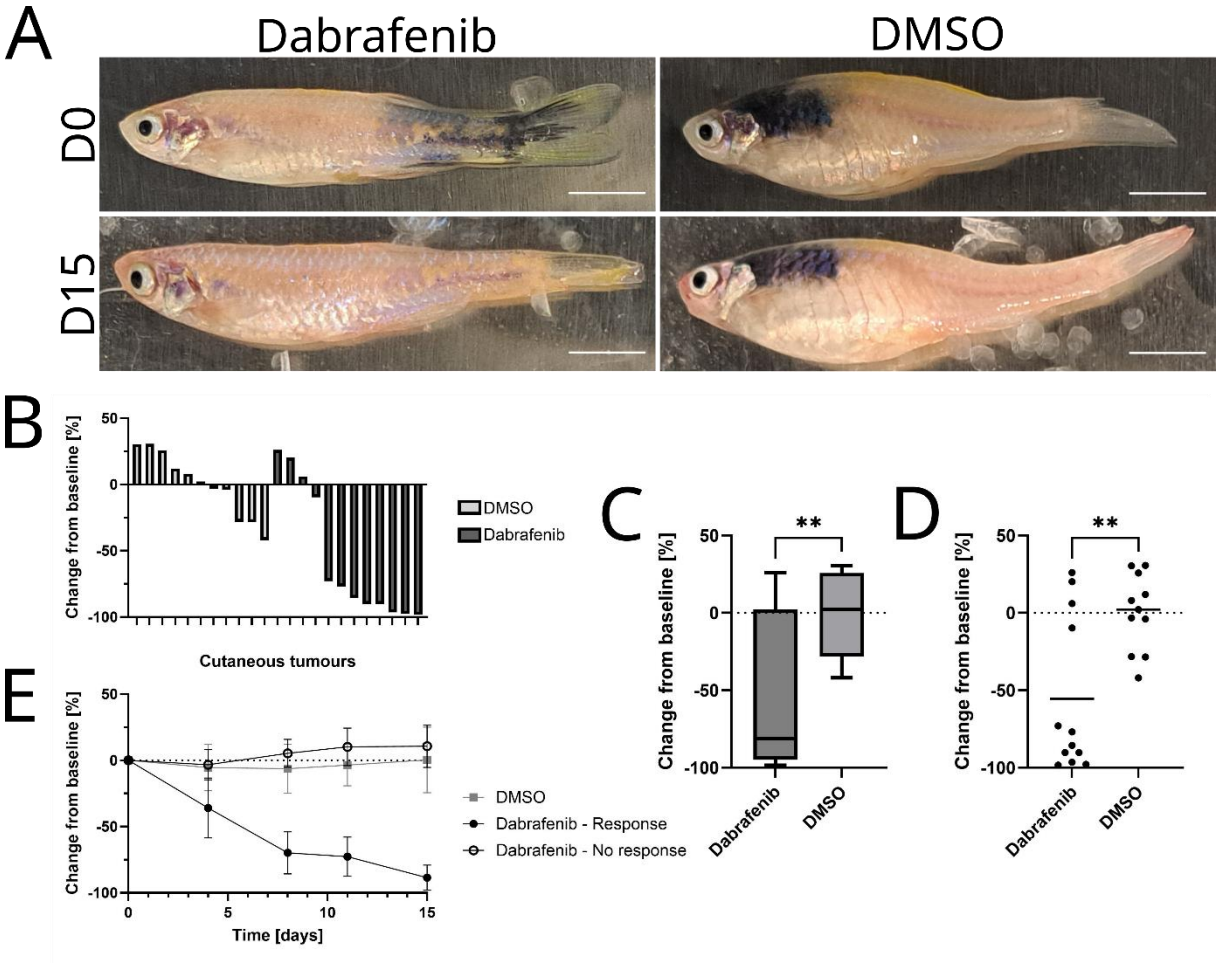

Figure 8. Cutaneous tumours in zebrafish during 2-week dabrafenib treatment. A. Representative images of zebrafish with BRAF V600E-mutated cutaneous tumours were taken on day 0 and day 15 of dabrafenib or control treatment. Scale bar = 5 mm. B. Waterfall plot presenting the change in percentage of the size of each cutaneous tumour during 2-week long dabrafenib treatment period. The change was calculated relative to baseline. Each bar represents one tumour. C. Boxplot summarizing the cutaneous melanoma size change in dabrafenib-treated and control groups. D. Scatter dot plot of cutaneous melanoma size change reveals responder and non-responder group. Individual data points represent tumours. E. The cutaneous tumour size change over time. The mean and SD are presented. Statistical tests have been performed using independent t-test, **p<0.01.

The difference between dabrafenib-treated and control fish was also observed with uveal melanoma (Figure 9A). The change in uveal tumour size was between -88.5% and -41.92% for dabrafenib treated fish and between -26.1% and +42.7% for control fish (Figure 9B). The mean change for treated fish was -67.5% (SD 22.6, n=5) and for control fish -6.9% (SD 19.2, n=5) (Figure 9C). The difference is statistically significant (p=0.0017). For the uveal melanoma, we did not observe separate responders and non-responders to dabrafenib treatment (Figure 9D). Overall, dabrafenib seemed to be effective

to treat cutaneous and uveal BRAF V600E-mutated melanoma in zebrafish. The size of the uveal tumours that responded to dabrafenib treatment decreased during the two-week experiment while the tumour of control fish stayed approximately the same size (Figure 9E).

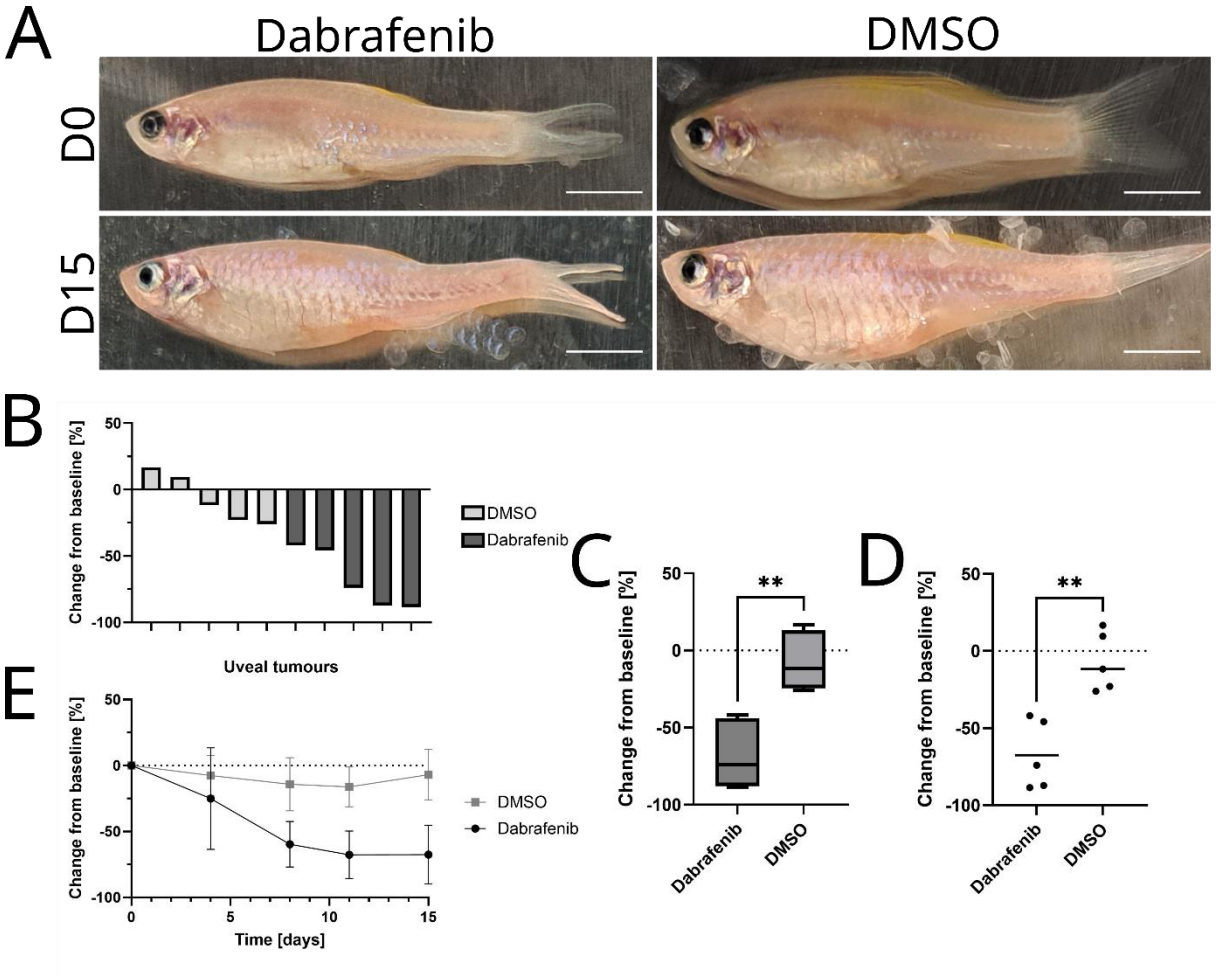

Figure 9. Uveal tumours in zebrafish during 2-week dabrafenib treatment. A. Representative images of zebrafish with BRAF V600E-mutated uveal tumours were taken on day 0 and day 15 of dabrafenib or control treatment. Scale bar = 5 mm. B. Waterfall plot presenting the change in percentage of the size of each uveal tumour during 2-week long dabrafenib treatment period. The change was calculated relative to baseline. Each bar represents one tumour. C. Boxplot summarizing the uveal melanoma size change in dabrafenib-treated and control groups. D. Scatter dot plot of uveal melanoma size change reveals responder and non-responder group. Individual data points represent tumours. E. The uveal tumour size change over time. The mean and SD are presented. Statistical tests have been performed using independent t-test, **p<0.01.

2.3.3 Histological changes

Histological analyses were performed to see changes between dabrafenib treated and untreated zebrafish on a cellular level. We did not observe any statistically significant differences between the groups. Skin melanomas were observable in both groups: 64% control fish (n=11) and 62% treated fish (n=13) (p>0.99, Figures 10B and 10F). However, the melanoma cells seemed to be lighter and reduced in number in treated fish.

Metastases were observed in 67% treated (n=12) and 29% untreated fish (n=7). The result was not statistically significant (p=0.17), but there was a notable difference in proportions. Most commonly melanoma cells had infiltrated into muscle (Figures 10C and 10F). Melanoma was also detectable in glandular structures (Figure 10C), spinal cord (Figures 10D) and brain (Figure 9G). The metastases seemed to be in the connective tissue surrounding organs even though for brain and spinal cord metastases, the melanoma cells had passed the bone. Although the melanoma had spread widely to the skin and muscle, it was not observed to spread to the internal organs.

Melanocyte eating macrophages, melanophages, were observable in 58% dabrafenib treated (n=12) and in 29% control fish (n=7) (Figure 10H). Although the difference between groups did not reach statistical significance (p=0.37), there might be a trend towards more melanophages in dabrafenib-treated group.

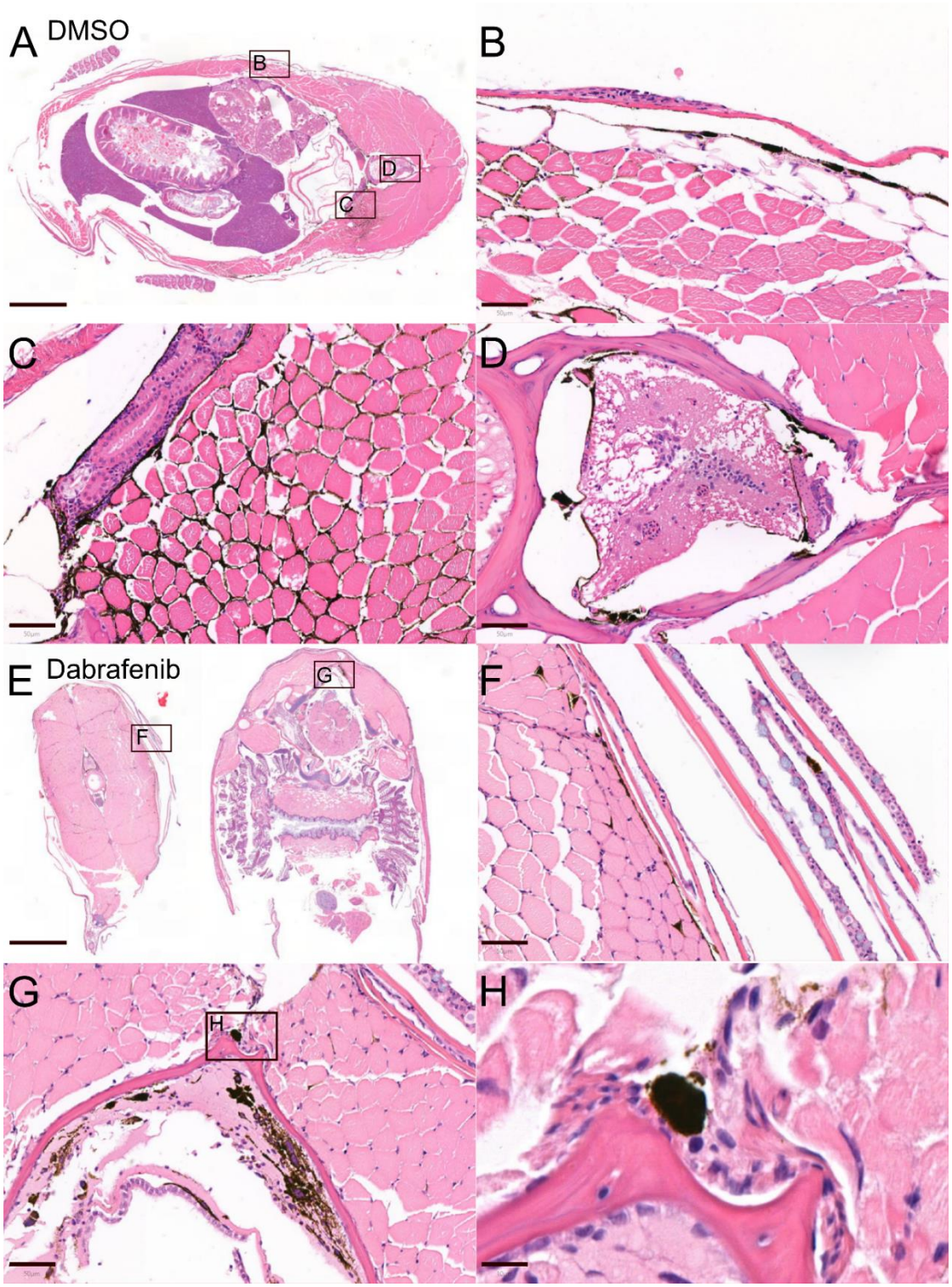

Figure 10. Histological cross-section of zebrafish with melanoma tumour. Haematoxylin & eosin staining was performed to visualize melanoma and the effects of dabrafenib-treatment on a cellular level. A. Cross-section of control fish with several areas of melanoma. B. Higher magnification image from panel A showing melanoma in skin and infiltered into muscle. C. Higher magnification image from panel A showing melanoma infiltered into muscle and glandular tissue. D. Higher magnification image from panel A showing melanoma infiltered into spinal cord. E. Cross-section of fish treated with dabrafenib with several melanoma areas. F. Higher magnification image from panel E showing melanoma in skin and infiltered into muscle. G. Higher magnification image from panel E showing melanoma infiltered into spinal cord. H. Higher magnification image from panel G showing melanophages (arrows) in the spinal cord. Scale bar = 800µm for panels A and E, 50µm for panels B-D and F-G, 10µm for panel H.

2.3.4 Mechanism of action

To prove dabrafenib's known mechanism of action, inhibition of MAPK pathway, we studied the expression of phosphorylated and non-phosphorylated ERK using Western blot (Figure 11A; full-length blots in Supplementary Figure 2). With higher dabrafenib concentrations phospho-ERK levels decreased dose-dependently. ERK levels stayed stable. Loading control β-actin showed similar protein loading to all wells. These results from three replicate Western blot studies were quantified (Figure 11B), and IC50 value of phosphorylated ERK was 72 nM (CI 95% 39-130 nM).

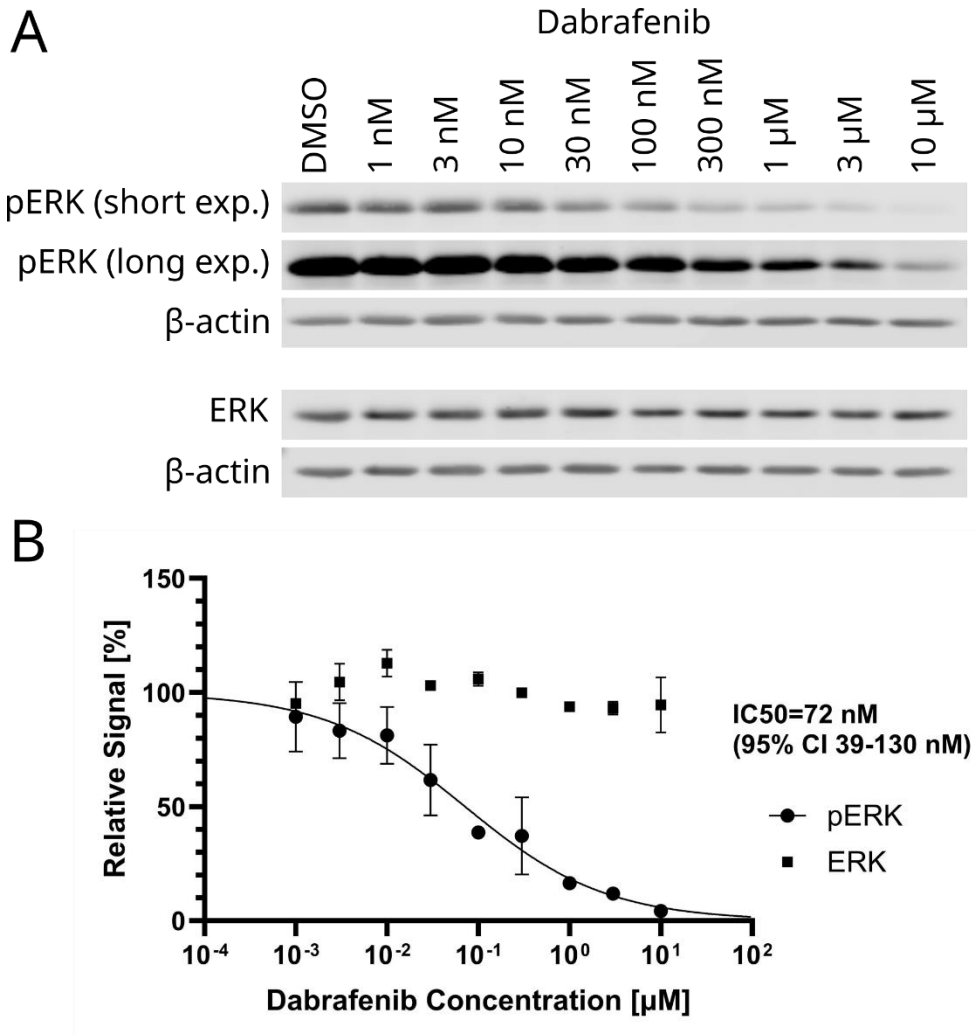

Figure 11. Western blot of total ERK and phosphorylated ERK with increasing dabrafenib concentrations. Protein lysates were extracted from ZMEL1-GFP cell treated with increasing dabrafenib concentrations (from 1 nM to 10 mM) and probed with antibodies against ERK and phospho-ERK. β-actin was used as a loading control. A. Representative immunoblot of ERK, phospho-ERK (pERK) and β-actin. The same phospho-ERK levels are shown with two different exposure times. B. Quantified Western blot of total ERK and phospho-ERK with increasing dabrafenib concentrations. Relative signal is calculated as the normalized value between phospho-ERK or ERK and β-actin. The mean and SEM of two replicate studies are presented.

To validate the *in vitro* observed reduction in ERK phosphorylation following dabrafenib treatment, we examined histological tissue sections *ex vivo*. We manually annotated the tumour region and identified the darkest area through threshold-based segmentation (Supplementary Figure 3). We did not observe any statistically significant difference in DAB staining of phosphorylated ERK (Figure 12A) or melanoma colour (Figure 12B) intensity between the dabrafenib-treated and control fish.

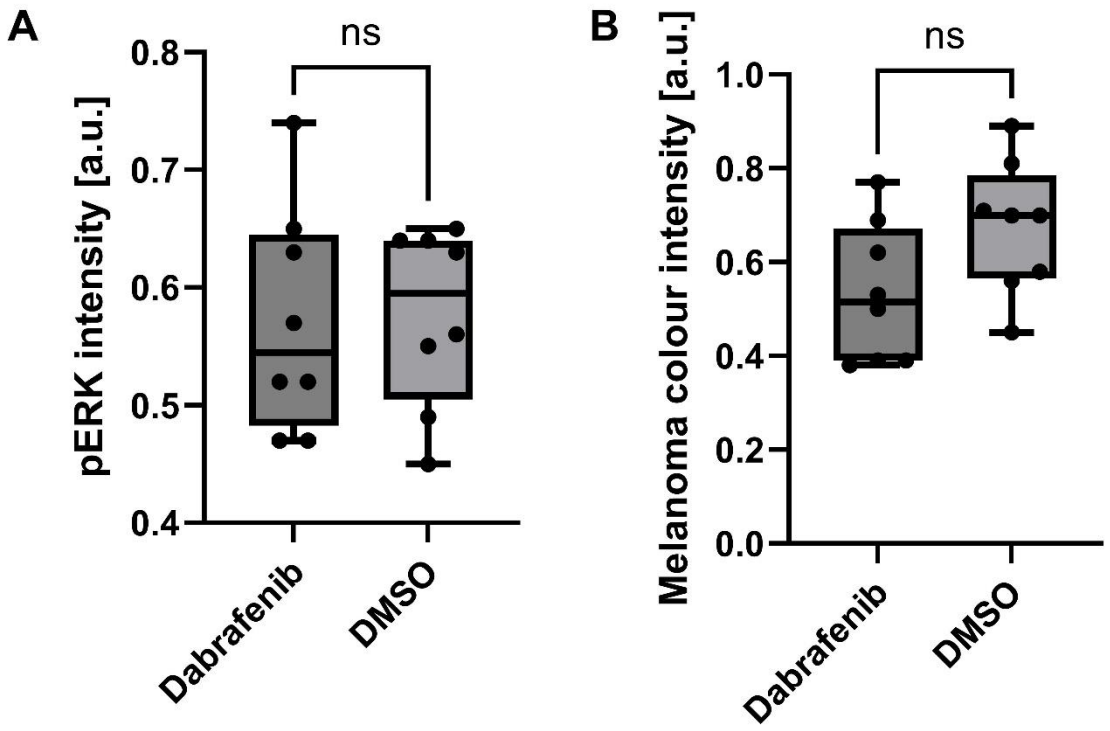

Figure 12. Quantification of phospho-ERK intensity with DAB staining intensity of histological sections. Brightfield images of tissue sections stained with DAB were analysed using colour deconvolution. The brown melanoma and pink DAB channels were isolated, and thresholding of brown channel was applied to quantify the positively stained area. A. Phospho-ERK (DAB) staining intensity. B. Tumour colour intensity. Statistical tests have been performed using independent t-test.

3 Discussion

3.1 Feasibility of the zebrafish melanoma model treated with tank water-administered dabrafenib

3.1.1 The BRAF V600E-mutated zebrafish melanoma model

In the study, we used the widely utilized BRAF V600E zebrafish melanoma model (Frantz and Ceol, 2020). The injection efficacy was low as only 2% of the injected embryos developed melanocytic hyperplasia at 3 dpi, and all neoplasias at the embryo stage did not develop into melanomas in adult fish. Other studies using the same BRAF V600E-mutated model have reported also low transfection efficacies of 6% at 4-months (Patton et al., 2005) and 10% at 3-months of age (Ceol et al., 2011). However, we chose the positive embryos based on pigmented melanoma cells instead of using GFP marker. Possibly the lightest positive cells would have been observed more sensitively using the fluorescence. It also took a more than half a year to develop tumours. The other studies using this model reported tumour development in 4-12-month-old zebrafish (Patton et al., 2005; White et al., 2011), which also indicated slow tumour development.

Melanomas were mainly observed in the skin but also in the eyes. The tumour sizes were easy to follow as they appeared dark pigmented. The tumours could grow to cover large areas of skin without affecting the health of the zebrafish. Through histology, we observed metastases in subcutaneous tissue, central nervous system and other internal organs, where metastases have also been observed in humans (Damsky et al., 2010). In zebrafish, it is impossible to study all common metastasis sites as zebrafish do not have, for example, lungs (Hason and Bartůněk, 2019). We also observed tumours originating from other pigment cells, xanthophores (Kelsh et al., 1996), which are absent in humans and therefore not in our interest. Overall, we found the BRAF V600E mutant zebrafish model feasible and behaviourally similar to human melanoma even though the transfection efficacy was low and tumours needed to develop several months.

3.1.2 Drug administration into tank water

Oral administration is the predominant route for delivering drugs to humans (Alqahtani et al., 2021). BRAF inhibitor vemurafenib has been administered to adult fish reaching therapeutic response by oral gavage and feeding pellets including the drug (Dang et al., 2016; Lu and Patton, 2022). However, these routes are impractical as gavage to small fish is challenging (Dang et al., 2016), and uptake through food is difficult to control (Lu and Patton, 2022), which can cause uneven dosing between

fish. In addition, the administration can be performed only a couple times a day, which makes the administration of drugs with short half-life impractical.

The waterborne exposure is often used for embryo or larvae stage zebrafish in pharmacological and toxicological studies, while in adult fish this administration route is more rarely used (Patton et al., 2021). Our study indicates that administration of dabrafenib via tank water is a feasible method as we assessed pharmacokinetics, metabolism and efficacy. All the fish have the same external exposure, and the administration is continuous. In the case of drugs with short half-life in zebrafish, such as dabrafenib, the administration into tank water may facilitate the effective therapeutic dose better throughout long-term treatment. However, pharmacological comparisons between different delivery routes in zebrafish are still needed.

3.2 Translatability of the zebrafish melanoma model treated with tank water-administered dabrafenib

3.2.1 Absorption and elimination kinetics

Dabrafenib added to the tank water was quickly absorbed and detectable in the plasma within half an hour of exposure. The plasma levels peaked at four hours. In humans the maximum concentration has been observed 2.0 hours post-exposure (Falchook et al., 2014). After the maximum serum concentration, the dabrafenib plasma levels started to decline reaching 2.7 μM (SD 2.3) at 24 hours post-exposure and 5.9 μM (SD 3.3) after 2 weeks. The phenomenon is similar to humans, where dabrafenib exposure decreases over time following repeated administration (Falchook et al., 2014). That and detection of hydroxy.dabrafenib soon after dabrafenib administration suggest active metabolism in zebrafish.

After discontinuing dabrafenib administration, dabrafenib and hydroxy-dabrafenib were cleared rapidly from zebrafish as the concentration started to decline steadily. Half-life of dabrafenib was 1.0 hours and of HDAB 1.6 hours. In humans, elimination half-life has been demonstrated to be 2.6 hours after intravenous administration and 4.8 hours after a single oral dose (Denton et al., 2013). The results demonstrate fast absorption and elimination kinetics of dabrafenib in zebrafish similar to humans with therapeutically relevant steady-state plasma levels.

As the sample size was small and deviation relatively large, we were unable to model absorption in more detail. Small serum sample size caused technical issues with analysis and affected the deviation. However, there was indication of complex absorption pharmacokinetics. In humans, sex and body

weight has but age does not have a statistically significant influence on dabrafenib pharmacokinetics even though they are found to be clinically irrelevant (Oullet et al., 2014). Because of the small sample size, we were unable to model the effect of these characteristics on plasma exposure in zebrafish.

3.2.2 Metabolites and distribution

In humans, dabrafenib is metabolized into hydroxy-dabrafenib, carboxy-dabrafenib and desmethyl-dabrafenib. We were able to detect dabrafenib and its hydroxy- and desmethyl-metabolites in zebrafish. However, we were unable to detect any carboxy-dabrafenib. Technical limitations of mass spectrometry imaging cannot be excluded, as carboxy-dabrafenib may undergo fast conversion to desmethyl-dabrafenib, which was detectable. These results indicate similar metabolism process in zebrafish as in humans.

The signal localization reflected the distribution of dabrafenib and its metabolites. Dabrafenib was widely distributed, while hydroxy-dabrafenib and desmethyl-dabrafenib were mainly located presumably in the gut. As dabrafenib and its metabolites are mainly extracted in bile and the metabolism of carboxy-dabrafenib into desmethyl-dabrafenib happens non-enzymatically in the gut (Bershas et al., 2013), our results were indicative of similar distribution. Dabrafenib signal was also observed in gills, which are possible an absorption and elimination route for zebrafish. Obviously, this differs from humans. We did not observe dabrafenib or its metabolites in brain or skeletal muscle. Brain exposure has been observed to be low also in humans (Mittapalli et al., 2013). In addition, we need to take the suboptimal sample integrity into consideration when interpreting these results.

There are differences between humans and zebrafish considering metabolism routes. In humans, the metabolism of dabrafenib and further metabolites is catalysed mainly by CYP3A4 and CYP2C8 enzymes (Bershas et al., 2013). Zebrafish have orthologous CYP enzymes, but their substrate specificity and expression differ from humans (Goldstone et al., 2010). Dabrafenib has also been demonstrated to activate the human pregnane X receptor (PXR) receptor, which induces CYPs and clearance over time through auto-induction (Creusot et al., 2020). Dabrafenib does not activate zebrafish PXR (Creusot et al., 2020), so the auto-induction loop is probably different or absent in zebrafish. This can modify the dabrafenib metabolism route.

3.2.3 Efficacy

Dabrafenib was found to be efficient in BRAF V600E-mutated zebrafish and ZMEL1-GFP cells. In cells, dabrafenib halts proliferation and often triggers apoptosis (King et al., 2013). We observed

dose-dependent decrease in the ZMEL1-GFP cell model with increasing dabrafenib concentrations with IC50 value of 90 nM. The IC50 value is well below the reached steady state dabrafenib plasma levels of 2.7 µM. Consistent with in vitro analysis, study in BRAF V600E-mutated zebrafish demonstrated robust efficacy *in vivo* with tank water-administered dabrafenib. The size of cutaneous tumours in the dabrafenib-treated group declined 56% (compared to +0.32% in control group) and the size of uveal tumours declined 68% (compared to -6.9% in control group). The differences could also be observed and followed clearly visually.

In our study, we observed responders and non-responders to the dabrafenib treatment with 67% response rate of cutaneous tumours. In clinical trials, the ORR was found to be 50% with dabrafenib treatment (Hauschild et al., 2012; Long et al., 2014), which was in line with our zebrafish efficacy study. Better response rate in zebrafish model can be due to multiple reasons. In our study, dabrafenib was delivered directly in the water which leads to continuous high local exposure. In zebrafish the tumours are less heterogenous and have more uniform drug sensitivity, while in humans the tumours have more diverse mutations due to cumulative sun damage (Yen et al., 2013). Response rates are also defined differently. In zebrafish response rate was measured by tumour size reduction during two weeks, while in clinical trials the ORR is defined differently, time period is longer and transient responses do not count (Hauschild et al., 2012; Long et al., 2014b).

Resistance is a huge problem with dabrafenib treatment in clinics (Hauschild et al., 2012; Zhong et al., 2022). Because all BRAF V600E-mutated tumours did not respond to the treatment, we can believe that zebrafish also develop resistance to dabrafenib treatment. The resistance mechanisms and their similarity should be studied in more detail. However, this gives us a reason to use zebrafish as a model to study the resistance of BRAF V600E-mutated melanoma in this model. Overall, dabrafenib seemed to be effective to treat cutaneous and uveal BRAF V600E-mutated melanoma in zebrafish.

3.2.4 Histological changes

Pigmented melanoma cells were observable in skin, muscle, glandular structures and central nervous system. Although some of the melanomas covered a large area of the skin, they were not metastases widely into the internal organs. In addition, melanin eating macrophages common to vertebrates, melanophages (Bjørgen and Koppang, 2024), could be observed.

We did not observe any statistically significant differences between the control and dabrafenib-treated groups considering number of observable melanomas in skin or metastases. This suggests that the

grouping for treatment was successful. The melanoma tumours seemed to be lighter and reduced in number of treated fish. There was no statistical significance between the control and dabrafenib treated groups considering the amount of melanophages, even though there might be a trend towards more melanophages in dabrafenib-treated group.

3.2.5 Mechanism of action

Dabrafenib inhibits mutated BRAF V600E kinase of MAPK pathway, which leads to downregulation ERK phosphorylation through blocked upstream MEK activity and results in cell death (King et al., 2013). The western blot analysis of phospho-ERK levels showed that dabrafenib potently suppresses MAPK signalling in ZMEL1-GFP cells with an IC50 value of 72 nM, which is well below the steady-state plasma concentration of 2.7 μM. We observed dose-dependent decrease in phospho-ERK levels with higher dabrafenib concentrations while ERK levels stayed stable. The result indicates that tank water-administered dabrafenib is able to suppress MAPK signalling in zebrafish similarly to humans.

We also did phospho-ERK immunohistochemistry to validate the results from cell studies. In these samples, we did not observe difference in phospho-ERK signalling comparing fish treated two weeks with dabrafenib and control fish. However, there are several possible reasons why the reduction in phospho-ERK was not observed in these samples. Clinically, phospho-ERK levels fluctuate dynamically and timing of biopsy relative to dose is crucial: If the biopsy is taken too early or too late relative to dabrafenib dosing, the window of maximal phospho-ERK suppression may be missed (Falchook et al., 2014). We had only a few samples that had only sparse pigmented cells. The pigment could also cover the phospho-ERK signal. In addition, there might have been issues in the protocol, such as over fixation, poor antigen retrieval, melanin removal procedure, lack of decent positive or negative controls and quantification limits. Taken together, our data suggest that dabrafenib is able to suppress MAPK signalling in BRAF V600E driven zebrafish melanoma.

3.3 Conclusions

The BRAF V600E mutant zebrafish melanoma model served as a robust model for studying melanoma drug dabrafenib's pharmacological properties in zebrafish. Dabrafenib behaved similarly in zebrafish than in humans considering its efficacy, mechanism of action and pharmacokinetics. Direct dabrafenib administration into tank water was a feasible and efficient delivery method for long-term treatment of zebrafish, and we anticipate that this administration method extends also to other small molecule drugs. This study proved that zebrafish could be used to study resistance and new therapies in the future. The findings of this study demonstrate that zebrafish can serve as a viable

model for studying the major problem with current melanoma therapies, drug resistance, and exploring new therapeutic strategies.

4 Materials and methods

4.1 Plasmid microinjection

Mitfa (-/-), *p53* (-/-) zebrafish were bred, and the embryos were collected the following morning. Embryos at 1-cell stage were microinjected with 2.3 nl of an injection mix containing 12.5 ng/µl miniCoopR BRAF-V600E-2A-EGFP plasmid, 12.5 ng/µl Tol2TP RNA, 150 mM KCl and phenol red in ultrapure water. Injections were performed using a Nanoject II injector (3-000-205A, Drummond). Glass needles were pulled from capillaries (TW100-4, World Precision Instruments Ltd., Sarasota, FL) using a PB-7 micropipette puller (Narishige, Tokyo, Japan). Following microinjection, embryos were maintained in E3 medium (5 mM NaCl, 0.17 mM KCl, 0.33 mM CaCl2, 0.33 mM MgSO4) supplemented with 50 U/ml penicillin-streptomycin (Gibco) at 28.5°C. At 1 dpi, 20 mg/ml pronase E (Cas: 9036-06-0, Merck) was added to the embryos. At 3dpi, embryos were screened for patches or individual dark melanocytes using a Leica MZ6 stereomicroscope (Leica Microsystems, Wetzlar, Germany).

4.2 Zebrafish husbandry

Zebrafish were maintained according to the standard protocols (Aleström, 2020). During experiments, 5-20-month-old adult fish were housed in 2-litre tanks and fed Gemma Micro 300 dry food once daily. All experimental procedures were approved by the Animal Experimental Board of the Regional State Administrative Agency for Southern Finland (ESAVI/2688/2020).

4.3 Pharmacokinetic analysis from blood samples

Adult zebrafish, housed 2-3 fish per 2-litre tank, were treated with 10µM dabrafenib (HY-14660, MedChemExpress) added directly to the tank water. Samples were taken from fish in different time points after administration (0, 0.5, 1, 2, 4, 8, 24 h and 2 weeks) for absorption kinetics and after withdrawal in fresh tank water (0, 0.5, 1, 2, 4, 8, 26 h) for elimination kinetics. Blood was collected following chemical euthanasia with 400 mg/l MS222 (Cas: 886-86-2, Sigma-Aldrich) by transecting the tail between caudal and anal fin using a steel blade (Swann-Morton). Tubes and pipette tips were coated with 0.5M EDTA (pH=8.5, Cas: 6381-92-6, VWR Chemicals) in milliQ-water and air-dried prior to use. Samples were centrifuged for 5 using a bench-top centrifuge, and plasma was transferred to fresh EDTA-coated tube. Plasma samples were snap-frozen on dry-ice and stored at -80°C freezer. The serum samples were analysed using LC-MS/MS by Scherf-Clavel laboratory in University of München, Germany.

4.4 Distribution analysis with mass spectrometry imaging

After terminal blood sample collection, zebrafish exposed to 10 µM dabrafenib for 24 h were snap-frozen with dry ice in iso-propanol (Cas: 67-63-0, Sigma-Aldrich) and stored at –80°C. For sectioning, each fish was embedded on its left side onto specimen disk with M-1 Embedding Matrix (Epredia) inside the cooled Leica CM1950 cryostat. The samples were cryosectioned at 15 µm thickness. Mass spectrometry imaging was performed by Turku Metabolomics Centre.

Following mass spectrometry imaging, the matrix was removed by incubating the slides in acetone (Cas: 67-64-1, Sigma-Aldrich) for 15 min. Slides were then rehydrated through ethanol series: twice in 100% ethanol, once in 70% ethanol and once in milliQ-water for 3 min. For haematoxylin-eosin staining, slides were immersed in Mayer's hematoxylin solution (Sigma-Aldrich) for 10 min, rinsed under running tap water for 10 min, and briefly washed in milliQ-water. Slides were then immersed in 96% ethanol for 30 s prior to eosin staining with alcoholic Eosin Y solution (HT110116, Sigma-Aldrich) for 45 s. The staining was followed by a 1 min wash in 96% ethanol and two 3 min washes in 100% ethanol. The slides were then cleared twice in xylene (Sigma-Aldrich) for 5min, mounted with DPX mountant for histology (Ref: 06522, Sigma-Aldrich) and coverslipped. The sections were scanned using a Pannoramic P1000 (3DHISTECH) slide scanner at 40x magnification.

4.5 Treatment experiment

The fish were housed in groups of 2-3 individuals for 16 days. DMSO (Cas: 67-68-5, Sigma-Aldrich) or 10 µM dabrafenib (HY-14660, MedChemExpress) was administered directly into the tank water. Three studies at separate times were conducted (total n=28). Fish were visually inspected daily, and water quality was monitored by measuring nitrogen and oxygen levels every third day. The fish were weighted and imaged on days 0, 4, 8, 11 and 15 under anaesthesia with 160 mg/l tricaine (Cas: 886-86-2, Sigma-Aldrich). At these time points, tank water and dabrafenib dosing were renewed. Imaging was performed using a mobile phone, capturing views from both lateral sides for each fish.

4.6 Histology and immunohistochemistry

Sample preparation, H&E staining and phospho-ERK immunohistochemistry were performed by the Histology Core Facility of the Institute of Biomedicine, University of Turku. Zebrafish treated with 0 µM or 10 µM dabrafenib for 2 weeks were fixed in 10% neutral buffered formalin, cut into cross-sections through the melanoma, decalcified, dehydrated through ascending alcohol series, cleared with xylene, and embedded into paraffin. Paraffin blocks were sectioned at 4 µm thickness, and

sections were deparaffinized with xylene followed by rehydration through descending ethanol series. Hematoxylin and eosin staining was performed using an automated stainer, Autostainer (Leica Biosystems), following standard protocols.

For immunohistochemistry, antigen retrieval was performed using Epitope retrieval solution (Leica Biosystems). Staining was conducted using a semi-automated Lab Vision autostainer (Epredia). To remove melanin, sections were treated with 3.5% H_2O_2 and 1% KOH for 10 min, followed by incubation with BrightDiluent pre-protein block (BD09-125, WellMed). Sections were incubated with phospho-p44/42 primary antibody (1:800, #4370, Cell Signalling Technology) for 60 min, then with BrightVision secondary antibody (DPVR110HRP, WellMed) for 30 min, and finally with detection reagent (Polydetector HRP Fuchsia, BSB0364, BioSB) for 10 min. Counterstaining was performed with Mayer's hematoxylin for 1 min. The slides were scanned using Pannoramic P1000 (3DHISTECH) slide scanner with 40x magnification.

4.7 Cell culture

The ZMEL1-GFP cells (Heilmann et al., 2015) were cultured in DMEM High glucose media (ECB7501L, Euroclone) supplemented with 10% fetal bovine serum (FBS) (Biowest), 200mM glutamine (Euroclone), and 100 U/ml Penicillin-100 ug/ml Streptomycin (Euroclone). Cells were maintained in a humidified incubator at 28°C with 5% CO_2. The cells were passaged and seeded for experiments once a week: Cells were detached using 0.25% Trypsin-EDTA (Gibco) at 28°C for 20 min, neutralized with complete medium, and centrifuged at 500 xg for 5 minutes before resuspension in fresh medium. Cell counting was assessed by adding an aliquot of cell suspension to an equal volume of 0.4% Trypan Blue Stain (Invitrogen) and using TC10 Automatic Cell Counter (Bio-Rad). The ZMEL1-GFP cells were granted by Dr. Richard White (Memorial Sloan Kettering Cancer Center).

4.8 Dose-response assay

ZMEL1-GFP cells were seeded into 96-well plates at a density of 5,000 cells per well and allowed to adhere for 24 h. Dabrafenib was added in triplicate at concentrations ranging from 1 nM to 10 µM using a HD D3000 Digital Dispenser (HP). After 72 h incubation, 30 µl of CellTiter-Glo Luminescent Cell Viability Assay Solution (Promega) was added to each well. Plates were incubated on a Certomat MO shaker at room temperature for 10 min in the dark. Luminescence was measured using an Agilent Biotek Cytation5 Cell Imaging Multimode Reader (AH diagnostics). Four replicate assays were performed.

4.9 Western blot

In three replicate studies, $5x10^6$ ZMEL1-GFP cells were seeded onto 10 cm dishes. After 24 h, cells were treated with dabrafenib (HY-14660, MedChemExpress) at concentrations ranging from 1 nM to10 µM and incubated for an additional 24 h. Cells were then collected by scraping into PBS, pelletted by centrifuging at 4°C for 5 min and lysed in lysis buffer (150 mM NaCl, 50 mM Tris pH 7.5, 0.4% Triton-X, 2 mM CaCl2, 2 mM MgCl2, 1 mM EDTA, 5 mM NaF in milliQ-water) supplemented with Halt Protease and Phosphatase Inhibitor Cocktail (Thermo Scientific) and Genius Nuclease (Santa Cruz Biotechnology). Lysates were incubated on ice for 30 min. Equal amounts of cell lysate and 50mM Tris with 2% SDS (pH 7.4) was added before boiling samples at 95°C for 5 min on a heating block (Grant BT3) before centrifuging them at 21,000 xg for 5 min. Protein concentrations were measured using Pierce BCA Protein Assay (Thermo Scientific) according to manufacturer's instructions and Synergy H1 Hybrid Reader (Biotek).

For each sample, 30 µg total protein was mixed with 6x Laemmli buffer and boiled at 95°C for 5 min. Proteins were resolved by SDS-PAGE using Mini-Protean Tetra system (Bio-Rad) and transferred onto nitrocellulose membranes using Power Pac 2000 (Bio-Rad). Membranes were washed with milliQ-water and blocked with 5% or milk in TBST (150 mM NaCl, 0.005% Tween-20, 10 mM Tris-HCl pH 7.5 in milliQ-water) for 30 min at room temperature. Primary antibody incubation was performed overnight at 4°C using either Phospho-p44/42 MAPK (Erk1/2) (Thr202/Tyr204) antibody (1:1000, 9101S, Cell Signaling Technology) or p44/42 MAPK (Erk1/2) antibody (1:1000, 9102S, Cell Signaling Technology) diluted in 5% BSA in TBST with 0.01% NaN_3. After three TBST washes, membranes were incubated with IRDye 800CW Goat anti-Rabbit secondary antibody (1:10 000, LI-COR) diluted in blocking buffer for 1.5 h at room temperature. Following three additional TBST washes, signals were detected using Odyssey CLx (LI-COR). For loading control detection, membranes were stripped with stripping buffer (25 mM glycine-HCl, 1% SDS, pH 2) for 20 min, reblocked in 5% milk in TBST, and incubated with monoclonal anti-β-actin antibody (1:1000, A2228, Sigma-Aldrich) followed by IRDye 680RD Donkey anti-Mouse secondary antibody (1:10 000, LI-COR).

4.10 Image analysis

The zebrafish images, and histological and immunohistochemistry slides were analysed using QuPath (0.3.2). Melanoma lesions from 2-week treatment experiment were quantified by measuring the area of pigmented tumours. Response was determined to be over 30% decrease from baseline. Matching

pre-, and post-treatment lesions were compared by calculating the relative percentage change based on the tumour are. Phospho-ERK stainings were analysed by annotating the area around the dark melanocytes, separating dark (pigmented melanoma) and purple (phosphor-ERK staining) channels and measuring their intensity. Analysis and quantification of Western blot images were carried out using Image Studio (Version 5.5). Phospho- ERK and ERK band intensities were measured and normalized to actin signal for each line.

4.11 Statistical methods

The statistical analyses were performed and graphs generated using GraphPad Prism (Version 10.4.1). Data is presented as mean ± standard deviation (SD) or standard error of the mean (SEM). For comparisons between two groups, independent t-test was used for continuous variables and Fisher's exact test for categorical variables. P-values less than 0.05 were considered statistically significant.

Nonlinear curve fitting of dabrafenib absorption and elimination values was performed with a one-phase association and decay. Dose-response and quantified Western blot data was fitted using a non-linear regression (inhibitor vs. normalized response, variable slope). Dose-response data was normalized to DMSO-treated control and Western blot data to beta-actin loading control. In addition, IC_{50}-values were defined. The fittings were conducted using a least-squares regression, and goodness of fit was evaluated by R^2 values. Confidence intervals (95%) were calculated for estimated parameters.

5 Acknowledgements

I want to express my deepest gratitudes to my supervisors, Ilkka Paatero and Kari Kurppa, for their invaluable guidance, support and patience throughout this thesis project. I am truly grateful to Nikol Dibus for her assistance with cell work. Special thanks to Ilia Evstafev from Turku Metabolomics Centre, Histology Core Facility and Scherf-Clavel laboratory in University of München. A warm thank you to Anna-Mari Haapanen-Saaristo for keeping me company in the office and providing honest feedback throughout the process. I am also grateful to my other colleagues for their helpful insights. Finally, I want to thank my family and friends for their encouragement, support and love during this journey.

6 Abbreviations

CDAB	carboxy-dabrafenib
CPI	Immune checkpoint inhibitor
CR	complete response
CRISPR	clustered regularly interspaced short palindromic repeats
CYP	cytochrome P450
DAB	dabrafenib
DDAB	desmethyl-dabrafenib
DoR	duration of response
dpf	days post fertilization
dpi	days post injection
DTIC	dacarbazine
EMA	European Medicines Agency
ERK	Extracellular signal regulated kinase
FDA	U.S. Food & Drug Administration
HDAB	hydroxy-dabrafenib
HR	hazard ratio
MAPK	mitogen-activated protein kinase
MITF	microphthalmia-associated transcription factor
NMSC	non-melanoma skin cancer
ORR	objective response rate
OS	overall survival
PFS	progression-free survival
pERK	phosphorylated extracellular signal regulated kinase
PR	partial response
TTR	time to response
zPDX	zebrafish patient-derived xenograft

7 References

Abbasi, N.R., H.M. Shaw, D.S. Rigel, R.J. Friedman, W.H. McCarthy, I. Osman, A.W. Kopf, and D. Polsky. 2004. Early diagnosis of cutaneous melanoma: revisiting the ABCD criteria. JAMA. 292:2771-2776. doi:10.1001/jama.292.22.2771.

Ablain, J., E.M. Durand, S. Yang, Y. Zhou, and L.I. Zon. 2015. A CRISPR/Cas9 vector system for tissue-specific gene disruption in zebrafish. *Dev. Cell*. 32:756–764. doi:10.1016/j.devcel.2015.01.032.

Aleström, P., L. D'Angelo, P.J. Midtlyng, D.F. Schorderet, S. Schulte-Merker, F. Sohm, and S. Warner. 2020. Zebrafish: Housing and husbandry recommendations. *Lab Anim*. 54:213–224. doi:10.1177/0023677219869037.

Allard-Coutu, A., B. Heller, and V. Francescutti. 2020. Surgical management of lymph nodes in melanoma. *Surg. Clin. North Am*. 100:71–90. doi:10.1016/j.suc.2019.09.002.

Alqahtani, M.S., M. Kazi, M.A. Alsenaidy, and M.Z. Ahmad. 2021. Advances in oral drug delivery. *Front. Pharmacol.* 12:618411. doi:10.3389/fphar.2021.618411.

Amaria R.N., A. Reuben, Z.A. Cooper, and J.A. Wargo. 2015. Update on use of aldesleukin for treatment of high-risk metastatic melanoma. *Immunotargets Ther.* 4:79-89. doi:10.2147/itt.s61590.

Andrews, L.P., A.R. Cillo, L. Karapetyan, J.M. Kirkwood, C.J. Workman, and D.A.A. Vignali. 2022. Molecular pathways and mechanisms of LAG3 in Cancer Therapy. *Clin. Cancer Res*. 28:5030–5039. doi:10.1158/1078-0432.ccr-21-2390.

Appleton, E., E.A. Chiocca, G. Ungerechts, A. Melcher, and R. Vile. 2025. Oncolytic viruses as anticancer agents: clinical progress and remaining challenges. *Lancet*. 406:1295–1312. doi:10.1016/s0140-6736(25)01206-1.

Arnold, M., D. Singh, M. Laversanne, J. Vignat, S. Vaccarella, F. Meheus, A.E. Cust, E. De Vries, D.C. Whiteman, and F. Bray. 2022. Global burden of cutaneous melanoma in 2020 and projections to 2040. *JAMA Dermatol*. 158:495-503. doi:10.1001/jamadermatol.2022.0160.

Ascierto, P.A., J.M. Kirkwood, J.-J. Grob, E. Simeone, A.M. Grimaldi, M. Maio, G. Palmieri, A. Testori, F.M. Marincola, and N. Mozzillo. 2012. The role of BRAF V600 mutation in melanoma. *J. Transl. Med*. 10:85. doi:10.1186/1479-5876-10-85.

Beadling, C., E. Jacobson-Dunlop, F.S. Hodi, C. Le, A. Warrick, J. Patterson, A. Town, A. Harlow, F. Cruz, S. Azar, B.P. Rubin, S. Muller, R. West, M.C. Heinrich, and C.L. Corless. 2008. *KIT* gene mutations and copy number in melanoma subtypes. *Clin. Cancer Res*. 14:6821–6828. doi:10.1158/1078-0432.ccr-08-0575.

Bershas, D.A., D. Ouellet, D.B. Mamaril-Fishman, N. Nebot, S.W. Carson, S.C. Blackman, R.A. Morrison, J.L. Adams, K.E. Jurusik, D.M. Knecht, P.D. Gorycki, and L.E. Richards-Peterson. 2013. Metabolism and disposition of oral dabrafenib in cancer patients: proposed participation of aryl nitrogen in carbon-carbon bond cleavage via decarboxylation following enzymatic oxidation. *Drug Metab. Disp*. 41:2215–2224. doi:10.1124/dmd.113.053785.

Berwick, M., I. Orlow, A.J. Hummer, B.K. Armstrong, A. Kricker, L.D. Marrett, R.C. Millikan, S.B. Gruber, H. Anton-Culver, R. Zanetti, R.P. Gallagher, T. Dwyer, T.R. Rebbeck, P.A. Kanetsky, K. Busam, L. From, U. Mujumdar, H. Wilcox, C.B. Begg, and The GEM Study Group. 2006. The prevalence of *CDKN2A* germ-line mutations and relative risk for cutaneous malignant melanoma: an international population-based study. *Cancer Epidemiol. Biomarkers Prev*. 15:1520–1525. doi:10.1158/1055-9965.epi-06-0270.

Bjørgen, H., and E.O. Koppang. 2024. The melano-macrophage: The black leukocyte of fish immunity. *Fish Shellfish Immunol*. 148:109523. doi:10.1016/j.fsi.2024.109523.

Blass, E., D.B. Keskin, C.R. Tu, C. Forman, A. Vanasse, H.E. Sax, B. Shim, V. Chea, N. Kim, I. Carulli, J. Southard, H. Lyu, W. Lu, M. Rickles-Young, A.B. Afeyan, O. Olive, A. Mehndiratta, H. Greenslade, K. Shetty, J. Baginska, I. Gomez Diaz, A. Nau, K.L. Pfaff, A. Gans, S. Ranasinghe, E.I. Buchbinder, T.A. Sussman, M.L. Insco, C.H. Yoon, S.J. Rodig, S.A. Shukla, S. Li, J.C. Aster, D.A. Braun, C. Cibulskis, N. Hacohen, D.S. Neuberg, A. Giobbie-Hurder, K.J. Livak, E.F. Fritsch, G. Oliveira, J.M. Simon, C.J. Wu, and P.A. Ott. 2025. A multi-adjuvant personal neoantigen vaccine generates potent immunity in melanoma. *Cell*. 188:5125-5141.e27. doi:10.1016/j.cell.2025.06.019.

Braicu, C., M. Buse, C. Busuioc, R. Drula, D. Gulei, L. Raduly, A. Rusu, A. Irimie, A.G. Atanasov, O. Slaby, C. Ionescu, and I. Berindan-Neagoe. 2019. A comprehensive review on MAPK: A promising therapeutic target in cancer. *Cancers*. 11:1618. doi:10.3390/cancers11101618.

Cadet, J., and T. Douki. 2018. Formation of UV-induced DNA damage contributing to skin cancer development. *Photochem. Photobiol. Sci*. 17:1816–1841. doi:10.1039/c7pp00395a.

Camp, E., and M. Lardelli. 2001. Tyrosinase gene expression in zebrafish embryos. *Dev. Genes and Evol*. 211:150–153. doi:10.1007/s004270000125.

Carlino, M.S., J. Larkin, and G.V. Long. 2021. Immune checkpoint inhibitors in melanoma. *Lancet*. 398:1002–1014. doi:10.1016/s0140-6736(21)01206-x.

Carnahan, J., P.J. Beltran, C. Babij, Q. Le, M.J. Rose, S. Vonderfecht, J.L. Kim, A.L. Smith, K. Nagapudi, M.A. Broome, M. Fernando, H. Kha, B. Belmontes, R. Radinsky, R. Kendall, and T.L. Burgess. 2010. Selective and potent Raf inhibitors paradoxically stimulate normal cell

proliferation and tumor growth. *Mol. Cancer Ther*. 9:2399–2410. doi:10.1158/1535-7163.mct-10-0181.

Carr, S., C. Smith, and J. Wernberg. 2020. Epidemiology and risk factors of melanoma. *Surg. Clin. North Am*. 100:1–12. doi:10.1016/j.suc.2019.09.005.

Ceol, C.J., Y. Houvras, J. Jane-Valbuena, S. Bilodeau, D.A. Orlando, V. Battisti, L. Fritsch, W.M. Lin, T.J. Hollmann, F. Ferré, C. Bourque, C.J. Burke, L. Turner, A. Uong, L.A. Johnson, R. Beroukhim, C.H. Mermel, M. Loda, S. Ait-Si-Ali, L.A. Garraway, R.A. Young, and L.I. Zon. 2011. The histone methyltransferase SETDB1 is recurrently amplified in melanoma and accelerates its onset. *Nature*. 471:513–517. doi:10.1038/nature09806.

Chapman, A., L. Fernandez del Ama, J. Ferguson, J. Kamarashev, C. Wellbrock, and A. Hurlstone. 2014. Heterogeneous tumor subpopulations cooperate to drive invasion. *Cell Rep*. 8:688–695. doi:10.1016/j.celrep.2014.06.045.

Chen, X., S. Habib, M. Alexandru, J. Chauhan, T. Evan, J.M. Troka, A. Rahimi, B. Esapa, T.J. Tull, W.Z. Ng, A. Fitzpatrick, Y. Wu, J.L.C. Geh, H. Lloyd-Hughes, L.C.G.F. Palhares, R. Adams, H.J. Bax, S. Whittaker, J. Jacków-Malinowska, and S.N. Karagiannis. 2024. Chondroitin sulfate proteoglycan 4 (CSPG4) as an emerging target for immunotherapy to treat melanoma. *Cancers*. 16:3260. doi:10.3390/cancers16193260.

Chen, X., Y. Li, T. Yao, and R. Jia. 2021. Benefits of zebrafish xenograft models in cancer research. *Front. Cell Dev. Biol.* 9:616551. doi:10.3389/fcell.2021.616551.

Cichorek, M., M. Wachulska, A. Stasiewicz, and A. Tymińska. 2013. Skin melanocytes: biology and development. *Postepy Dermatol. Alergol*. 1:30–41. doi:10.5114/pdia.2013.33376.

Cilluffo, D., V. Barra, and A. Di Leonardo. 2020. $P14^{ARF}$: The Absence that makes the difference. *Genes*. 11:824. doi:10.3390/genes11070824.

Cockburn, M., S.M. Swetter, D. Peng, T.H.M. Keegan, D. Deapen, and C.A. Clarke. 2008. Melanoma underreporting: Why does it happen, how big is the problem, and how do we fix it? *J. Am. Acad. Dermatol*. 59:1081–1085. doi:10.1016/j.jaad.2008.08.007.

Conforti, C., and I. Zalaudek. 2021. Epidemiology and risk factors of melanoma: A review. *Dermatol. Pract. Concept*. 11:e2021161S. doi:10.5826/dpc.11s1a161s.

Creusot, N., M. Gassiot, E. Alaterre, B. Chiavarina, M. Grimaldi, A. Boulahtouf, L. Toporova, S. Gerbal-Chaloin, M. Daujat-Chavanieu, A. Matheux, R. Rahmani, C. Gongora, A. Evrard, P. Pourquier, and P. Balaguer. 2020. The anti-cancer drug dabrafenib is a potent activator of the human pregnane X receptor. *Cells*. 9:1641. doi:10.3390/cells9071641.

Cronin, J.C., J. Wunderlich, S.K. Loftus, T.D. Prickett, X. Wei, K. Ridd, S. Vemula, A.S. Burrell, N.S. Agrawal, J.C. Lin, C.E. Banister, P. Buckhaults, S.A. Rosenberg, B.C. Bastian, W.J.

Pavan, and Y. Samuels. 2009. Frequent mutations in the MITF pathway in melanoma. *Pigment Cell Melanoma Res*. 22:435–444. doi:10.1111/j.1755-148x.2009.00578.x.

Czarnecka, A.M., E. Bartnik, M. Fiedorowicz, and P. Rutkowski. 2020. Targeted therapy in melanoma and mechanisms of resistance. *Int. J. Mol. Sci*. 21:4576. doi:10.3390/ijms21134576.

Damsky, W.E., L.E. Rosenbaum, and M. Bosenberg. 2010. Decoding melanoma metastasis. *Cancers*. 3:126–163. doi:10.3390/cancers3010126.

Dang, M., R.E. Henderson, L.A. Garraway, and L.I. Zon. 2016. Long-term drug administration in the adult zebrafish using oral gavage for cancer preclinical studies. *Dis. Model. Mech*. 9:811-820. doi:10.1242/dmm.024166.

Davies, H., G.R. Bignell, C. Cox, P. Stephens, S. Edkins, S. Clegg, J. Teague, H. Woffendin, M.J. Garnett, W. Bottomley, N. Davis, E. Dicks, R. Ewing, Y. Floyd, K. Gray, S. Hall, R. Hawes, J. Hughes, V. Kosmidou, A. Menzies, C. Mould, A. Parker, C. Stevens, S. Watt, S. Hooper, R. Wilson, H. Jayatilake, B.A. Gusterson, C. Cooper, J. Shipley, D. Hargrave, K. Pritchard-Jones, N. Maitland, G. Chenevix-Trench, G.J. Riggins, D.D. Bigner, G. Palmieri, A. Cossu, A. Flanagan, A. Nicholson, J.W.C. Ho, S.Y. Leung, S.T. Yuen, B.L. Weber, H.F. Seigler, T.L. Darrow, H. Paterson, R. Marais, C.J. Marshall, R. Wooster, M.R. Stratton, and P.A. Futreal. 2002. Mutations of the *BRAF* gene in human cancer. *Nature*. 417:949–954. doi:10.1038/nature00766.

De Braud, F., C. Dooms, R.S. Heist, C. Lebbe, M. Wermke, A. Gazzah, D. Schadendorf, P. Rutkowski, J. Wolf, P.A. Ascierto, I. Gil-Bazo, S. Kato, M. Wolodarski, M. McKean, E. Muñoz Couselo, M. Sebastian, A. Santoro, V. Cooke, L. Manganelli, K. Wan, A. Gaur, J. Kim, G. Caponigro, X.-M. Couillebault, H. Evans, C.D. Campbell, S. Basu, M. Moschetta, and A. Daud. 2023. Initial evidence for the efficacy of naporafenib in combination with trametinib in *NRAS*-mutant melanoma: Results from the expansion arm of a phase Ib, open-label study. *J. Clin. Oncol*. 41:2651–2660. doi:10.1200/jco.22.02018.

De Pinto, G., S. Mignozzi, C. La Vecchia, F. Levi, E. Negri, and C. Santucci. 2024. Global trends in cutaneous malignant melanoma incidence and mortality. *Melanoma Res*. 34:265–275. doi:10.1097/cmr.0000000000000959.

Denton, C.L., E. Minthorn, S.W. Carson, G.C. Young, L.E. Richards-Peterson, J. Botbyl, C. Han, R.A. Morrison, S.C. Blackman, and D. Ouellet. 2013. Concomitant oral and intravenous pharmacokinetics of dabrafenib, a BRAF inhibitor, in patients with BRAF V600 mutation-positive solid tumors. *J. Clin. Pharmacol*. 53:955–961. doi:10.1002/jcph.127.

Dovey, M., R.M. White, and L.I. Zon. 2009. Oncogenic NRAS cooperates with *p53* loss to generate melanoma in zebrafish. *Zebrafish*. 6:397–404. doi:10.1089/zeb.2009.0606.

Dummer, R., P.A. Ascierto, H.J. Gogas, A. Arance, M. Mandala, G. Liszkay, C. Garbe, D. Schadendorf, I. Krajsova, R. Gutzmer, V. Chiarion-Sileni, C. Dutriaux, J.W.B. De Groot, N. Yamazaki, C. Loquai, L.A. Moutouh-de Parseval, M.D. Pickard, V. Sandor, C. Robert, and K.T. Flaherty. 2018. Encorafenib plus binimetinib versus vemurafenib or encorafenib in patients with *BRAF*-mutant melanoma (COLUMBUS): a multicentre, open-label, randomised phase 3 trial. *Lancet Oncol*. 19:603–615. doi:10.1016/s1470-2045(18)30142-6.

El Sharouni, M.-A., P.J. Van Diest, A.J. Witkamp, V. Sigurdsson, and C.H. Van Gils. 2020. Subtyping cutaneous melanoma matters. *JNCI Cancer Spectr*. 4:pkaa097. doi:10.1093/jncics/pkaa097.

European Medicines Agency. 2013. Summary of product characteristics: Tafinlar (dabrafenib). https://www.ema.europa.eu/en/documents/product-information/tafinlar-epar-product-information_en.pdf (accessed September 9, 2025).

Falchook, G.S., G.V. Long, R. Kurzrock, K.B. Kim, H.-T. Arkenau, M.P. Brown, O. Hamid, J.R. Infante, M. Millward, A. Pavlick, M.T. Chin, S.J. O'Day, S.C. Blackman, C.M. Curtis, P. Lebowitz, B. Ma, D. Ouellet, and R.F. Kefford. 2014. Dose selection, pharmacokinetics, and pharmacodynamics of BRAF Inhibitor dabrafenib (GSK2118436). *Clin. Cancer Res*. 20:4449–4458. doi:10.1158/1078-0432.ccr-14-0887.

Ferlay J, M. Ervik, F. Lam, M. Laversanne, M. Colombet, L. Mery, M. Piñeros, A. Znaor, I. Soerjomataram, F. Bray (2024). Global Cancer Observatory: Cancer Today. Lyon, France: International Agency for Research on Cancer. https://gco.iarc.who.int/today (accessed October 5, 2025).

Ferrucci, P.F., L. Pala, F. Conforti, and E. Cocorocchio. 2021. Talimogene laherparepvec (T-VEC): An intralesional cancer immunotherapy for advanced melanoma. *Cancers*. 13:1383. doi:10.3390/cancers13061383.

Frantz, W.T., and C.J. Ceol. 2020. From tank to treatment: Modeling melanoma in zebrafish. *Cells*. 9:1289. doi:10.3390/cells9051289.

Gabellini, C., E. Gómez-Abenza, S. Ibáñez-Molero, M.G. Tupone, A.B. Pérez-Oliva, S. De Oliveira, D. Del Bufalo, and V. Mulero. 2018. Interleukin 8 mediates bcl-xL-induced enhancement of human melanoma cell dissemination and angiogenesis in a zebrafish xenograft model. *Int. J. Cancer*. 142:584–596. doi:10.1002/ijc.31075.

Gainor, J.F., M.R. Patel, J.S. Weber, M. Gutierrez, J.E. Bauman, J.M. Clarke, R. Julian, A.J. Scott, J.L. Geiger, K. Kirtane, C. Robert-Tissot, B. Coder, M. Tasneem, J. Sun, W. Zheng, L.

Gerbereux, A. Laino, F. Porichis, J.R. Pollard, P. Hou, V. Sehgal, X. Chen, M. Morrissey, H.N. Daghestani, I. Feldman, L. Srinivasan, J.P. Frederick, M. Brown, P. Aanur, R. Meehan, and H.A. Burris. 2024. T-cell responses to individualized neoantigen therapy mRNA-4157 (V940) alone or in combination with pembrolizumab in the phase 1 KEYNOTE-603 study. *Cancer Discov*. 14:2209–2223. doi:10.1158/2159-8290.cd-24-0158.

Garraway, L.A., H.R. Widlund, M.A. Rubin, G. Getz, A.J. Berger, S. Ramaswamy, R. Beroukhim, D.A. Milner, S.R. Granter, J. Du, C. Lee, S.N. Wagner, C. Li, T.R. Golub, D.L. Rimm, M.L. Meyerson, D.E. Fisher, and W.R. Sellers. 2005. Integrative genomic analyses identify *MITF* as a lineage survival oncogene amplified in malignant melanoma. *Nature*. 436:117–122. doi:10.1038/nature03664.

Goel, V.K., A.J.F. Lazar, C.L. Warneke, M.S. Redston, and F.G. Haluska. 2006. Examination of mutations in BRAF, NRAS, and PTEN in primary cutaneous melanoma. *J. Invest. Dermatol*. 126:154–160. doi:10.1038/sj.jid.5700026.

Goldstone, J.V., A.G. McArthur, A. Kubota, J. Zanette, T. Parente, M.E. Jönsson, D.R. Nelson, and J.J. Stegeman. 2010. Identification and developmental expression of the full complement of Cytochrome P450 genes in Zebrafish. *BMC Genomics*. 11:643. doi:10.1186/1471-2164-11-643.

Guo, W., H. Wang, and C. Li. 2021. Signal pathways of melanoma and targeted therapy. *Signal Transduct. Target. Ther*. 6:424. doi:10.1038/s41392-021-00827-6.

Haldi, M., C. Ton, W.L. Seng, and P. McGrath. 2006. Human melanoma cells transplanted into zebrafish proliferate, migrate, produce melanin, form masses and stimulate angiogenesis in zebrafish. *Angiogenesis*. 9:139–151. doi:10.1007/s10456-006-9040-2.

Hartman, M.L., and M. Czyz. 2015. MITF in melanoma: mechanisms behind its expression and activity. *Cell. Mol. Life Sci.* 72:1249–1260. doi:10.1007/s00018-014-1791-0.

Hason, M., and P. Bartůněk. 2019. Zebrafish models of cancer—New insights on modeling human cancer in a non-mammalian vertebrate. *Genes*. 10:935. doi:10.3390/genes10110935.

Hatzivassiliou, G., K. Song, I. Yen, B.J. Brandhuber, D.J. Anderson, R. Alvarado, M.J.C. Ludlam, D. Stokoe, S.L. Gloor, G. Vigers, T. Morales, I. Aliagas, B. Liu, S. Sideris, K.P. Hoeflich, B.S. Jaiswal, S. Seshagiri, H. Koeppen, M. Belvin, L.S. Friedman, and S. Malek. 2010. RAF inhibitors prime wild-type RAF to activate the MAPK pathway and enhance growth. *Nature*. 464:431–435. doi:10.1038/nature08833.

Hauschild, A., P.A. Ascierto, D. Schadendorf, J.J. Grob, A. Ribas, F. Kiecker, C. Dutriaux, L.V. Demidov, C. Lebbé, P. Rutkowski, C.U. Blank, R. Gutzmer, M. Millward, R. Kefford, T. Haas, A. D'Amelio, E. Gasal, B. Mookerjee, and P.B. Chapman. 2020. Long-term outcomes

in patients with *BRAF* V600-mutant metastatic melanoma receiving dabrafenib monotherapy: Analysis from phase 2 and 3 clinical trials. *Eur. J. Cancer*. 125:114–120. doi:10.1016/j.ejca.2019.10.033.

Hauschild, A., J.-J. Grob, L.V. Demidov, T. Jouary, R. Gutzmer, M. Millward, P. Rutkowski, C.U. Blank, W.H. Miller, E. Kaempgen, S. Martín-Algarra, B. Karaszewska, C. Mauch, V. Chiarion-Sileni, A.-M. Martin, S. Swann, P. Haney, B. Mirakhur, M.E. Guckert, V. Goodman, and P.B. Chapman. 2012. Dabrafenib in *BRAF*-mutated metastatic melanoma: a multicentre, open-label, phase 3 randomised controlled trial. *Lancet*. 380:358–365. doi:10.1016/s0140-6736(12)60868-x.

Hawkes, J.W. 1974. The structure of fish skin: I. General organization. *Cell Tissue Res.* 149:147–158. doi:10.1007/bf00222270.

Heidorn, S.J., C. Milagre, S. Whittaker, A. Nourry, I. Niculescu-Duvas, N. Dhomen, J. Hussain, J.S. Reis-Filho, C.J. Springer, C. Pritchard, and R. Marais. 2010. Kinase-dead BRAF and oncogenic RAS cooperate to drive tumor progression through CRAF. *Cell*. 140:209–221. doi:10.1016/j.cell.2009.12.040.

Heilmann, S., K. Ratnakumar, E.M. Langdon, E.R. Kansler, I.S. Kim, N.R. Campbell, E.B. Perry, A.J. McMahon, C.K. Kaufman, E. Van Rooijen, W. Lee, C.A. Iacobuzio-Donahue, R.O. Hynes, L.I. Zon, J.B. Xavier, and R.M. White. 2015. A quantitative system for studying metastasis using transparent zebrafish. *Cancer Res*. 75:4272–4282. doi:10.1158/0008-5472.can-14-3319.

Henrikson, R.C., and A.G. Matoltsy. 1967. The fine structure of teleost epidermis. *J. Ultrastruct. Res*. 21:194–212. doi:10.1016/s0022-5320(67)80091-1.

Hirata, M., K. Nakamura, T. Kanemaru, Y. Shibata, and S. Kondo. 2003. Pigment cell organization in the hypodermis of zebrafish. *Dev. Dyn*. 227:497–503. doi:10.1002/dvdy.10334.

Hodis, E., I.R. Watson, G.V. Kryukov, S.T. Arold, M. Imielinski, J.-P. Theurillat, E. Nickerson, D. Auclair, L. Li, C. Place, D. DiCara, A.H. Ramos, M.S. Lawrence, K. Cibulskis, A. Sivachenko, D. Voet, G. Saksena, N. Stransky, R.C. Onofrio, W. Winckler, K. Ardlie, N. Wagle, J. Wargo, K. Chong, D.L. Morton, K. Stemke-Hale, G. Chen, M. Noble, M. Meyerson, J.E. Ladbury, M.A. Davies, J.E. Gershenwald, S.N. Wagner, D.S.B. Hoon, D. Schadendorf, E.S. Lander, S.B. Gabriel, G. Getz, L.A. Garraway, and L. Chin. 2012. A landscape of driver mutations in melanoma. *Cell*. 150:251–263. doi:10.1016/j.cell.2012.06.024.

Hossain, S.M., and M.R. Eccles. 2023. Phenotype switching and the melanoma microenvironment; Impact on immunotherapy and drug resistance. *Int. J. Mol. Sci*. 24:1601. doi:10.3390/ijms24021601.

Howe, K., M.D. Clark, C.F. Torroja, J. Torrance, C. Berthelot, M. Muffato, J.E. Collins, S. Humphray, K. McLaren, L. Matthews, S. McLaren, I. Sealy, M. Caccamo, C. Churcher, C. Scott, J.C. Barrett, R. Koch, G.-J. Rauch, S. White, W. Chow, B. Kilian, L.T. Quintais, J.A. Guerra-Assunção, Y. Zhou, Y. Gu, J. Yen, J.-H. Vogel, T. Eyre, S. Redmond, R. Banerjee, J. Chi, B. Fu, E. Langley, S.F. Maguire, G.K. Laird, D. Lloyd, E. Kenyon, S. Donaldson, H. Sehra, J. Almeida-King, J. Loveland, S. Trevanion, M. Jones, M. Quail, D. Willey, A. Hunt, J. Burton, S. Sims, K. McLay, B. Plumb, J. Davis, C. Clee, K. Oliver, R. Clark, C. Riddle, D. Elliott, G. Threadgold, G. Harden, D. Ware, S. Begum, B. Mortimore, G. Kerry, P. Heath, B. Phillimore, A. Tracey, N. Corby, M. Dunn, C. Johnson, J. Wood, S. Clark, S. Pelan, G. Griffiths, M. Smith, R. Glithero, P. Howden, N. Barker, C. Lloyd, C. Stevens, J. Harley, K. Holt, G. Panagiotidis, J. Lovell, H. Beasley, C. Henderson, D. Gordon, K. Auger, D. Wright, J. Collins, C. Raisen, L. Dyer, K. Leung, L. Robertson, K. Ambridge, D. Leongamornlert, S. McGuire, R. Gilderthorp, C. Griffiths, D. Manthravadi, et al. 2013. The zebrafish reference genome sequence and its relationship to the human genome. *Nature*. 496:498–503. doi:10.1038/nature12111.

Hyenne, V., S. Ghoroghi, M. Collot, J. Bons, G. Follain, S. Harlepp, B. Mary, J. Bauer, L. Mercier, I. Busnelli, O. Lefebvre, N. Fekonja, M.J. Garcia-Leon, P. Machado, F. Delalande, A.A. López, S.G. Silva, F.J. Verweij, G. Van Niel, F. Djouad, H. Peinado, C. Carapito, A.S. Klymchenko, and J.G. Goetz. 2019. Studying the fate of tumor extracellular vesicles at high spatiotemporal resolution using the zebrafish embryo. *Dev. Cell*. 48:554-572.e7. doi:10.1016/j.devcel.2019.01.014.

Ilieva, K.M., I. Correa, D.H. Josephs, P. Karagiannis, I.U. Egbuniwe, M.J. Cafferkey, J.F. Spicer, M. Harries, F.O. Nestle, K.E. Lacy, and S.N. Karagiannis. 2014. Effects of *BRAF* mutations and *BRAF* inhibition on immune responses to melanoma. *Mol. Cancer Ther*. 13:2769–2783. doi:10.1158/1535-7163.mct-14-0290.

Janku, F., S. Bauer, K. Shoumariyeh, R.L. Jones, A. Spreafico, J. Jennings, C. Psoinos, J. Meade, R. Ruiz-Soto, and P. Chi. 2022. Efficacy and safety of ripretinib in patients with *KIT*-altered metastatic melanoma. *ESMO Open*. 7:100520. doi:10.1016/j.esmoop.2022.100520.

Javed, S.A., A. Najmi, W. Ahsan, and K. Zoghebi. 2024. Targeting PD-1/PD-L-1 immune checkpoint inhibition for cancer immunotherapy: success and challenges. *Front. Immunol.* 15:1383456. doi:10.3389/fimmu.2024.1383456.

Jiang, M., K. Zhang, Z. Zhang, X. Zeng, Z. Huang, P. Qin, Z. Xie, X. Cai, M. Ashrafizadeh, Y. Tian, and R. Wei. 2025. PI3K/AKT/mTOR axis in cancer: From pathogenesis to treatment. *MedComm*. 6:e70295. doi:10.1002/mco2.70295.

Kawakami, K., A. Shima, and N. Kawakami. 2000. Identification of a functional transposase of the *Tol2* element, an *Ac* -like element from the Japanese medaka fish, and its transposition in the zebrafish germ lineage. *Proc. Natl. Acad. Sci. U.S.A.* 97:11403–11408. doi:10.1073/pnas.97.21.11403.

Kelsh, R.N., M. Brand, Y.-J. Jiang, C.-P. Heisenberg, S. Lin, P. Haffter, J. Odenthal, M.C. Mullins, F.J.M.V. Eeden, M. Furutani-Seiki, M. Granato, M. Hammerschmidt, D.A. Kane, R.M. Warga, D. Beuchle, L. Vogelsang, and C. Nüsslein-Volhard. 1996. Zebrafish pigmentation mutations and the processes of neural crest development. *Development*. 123:369–389. doi:10.1242/dev.123.1.369.

Kichloo, A., M. Albosta, D. Dahiya, J.C. Guidi, M. Aljadah, J. Singh, H. Shaka, F. Wani, A. Kumar, and M. Lekkala. 2021. Systemic adverse effects and toxicities associated with immunotherapy: A review. *World J. Clin. Oncol*. 12:150–163. doi:10.5306/wjco.v12.i3.150.

Kim, I.S., S. Heilmann, E.R. Kansler, Y. Zhang, M. Zimmer, K. Ratnakumar, R.L. Bowman, T. Simon-Vermot, M. Fennell, R. Garippa, L. Lu, W. Lee, T. Hollmann, J.B. Xavier, and R.M. White. 2017. Microenvironment-derived factors driving metastatic plasticity in melanoma. *Nat. Commun*. 8:14343. doi:10.1038/ncomms14343.

Kimmel, C.B., W.W. Ballard, S.R. Kimmel, B. Ullmann, and T.F. Schilling. 1995. Stages of embryonic development of the zebrafish. *Dev. Dyn*. 203:253–310. doi:10.1002/aja.1002030302.

King, A.J., M.R. Arnone, M.R. Bleam, K.G. Moss, J. Yang, K.E. Fedorowicz, K.N. Smitheman, J.A. Erhardt, A. Hughes-Earle, L.S. Kane-Carson, R.H. Sinnamon, H. Qi, T.R. Rheault, D.E. Uehling, and S.G. Laquerre. 2013. Dabrafenib; preclinical characterization, increased efficacy when combined with trametinib, while BRAF/MEK tool combination reduced skin lesions. *PLoS One*. 8:e67583. doi:10.1371/journal.pone.0067583.

Krens, S.F.G., S. He, H.P. Spaink, and B.E. Snaar-Jagalska. 2006. Characterization and expression patterns of the MAPK family in zebrafish. *Gene Expr. Patterns*. 6:1019–1026. doi:10.1016/j.modgep.2006.04.008.

Kumar, R., S. Angelini, E. Snellman, and K. Hemminki. 2004. *BRAF* mutations are common somatic events in melanocytic nevi. *J. Invest. Dermatol*. 122:342–348. doi:10.1046/j.0022-202x.2004.22225.x.

Lam, S.H., H.L. Chua, Z. Gong, T.J. Lam, and Y.M. Sin. 2004. Development and maturation of the immune system in zebrafish, *Danio rerio*: a gene expression profiling, in situ hybridization and immunological study. *Dev. Comp. Immunol*. 28:9–28. doi:10.1016/s0145-305x(03)00103-4.

Langenau, D.M., A.A. Ferrando, D. Traver, J.L. Kutok, J.-P.D. Hezel, J.P. Kanki, L.I. Zon, A.T. Look, and N.S. Trede. 2004. *In vivo* tracking of T cell development, ablation, and engraftment in transgenic zebrafish. *Proc. Natl. Acad. Sci. U.S.A.* 101:7369–7374. doi:10.1073/pnas.0402248101.

Larkin, J., P.A. Ascierto, B. Dréno, V. Atkinson, G. Liszkay, M. Maio, M. Mandalà, L. Demidov, D. Stroyakovskiy, L. Thomas, L. De La Cruz-Merino, C. Dutriaux, C. Garbe, M.A. Sovak, I. Chang, N. Choong, S.P. Hack, G.A. McArthur, and A. Ribas. 2014. Combined vemurafenib and cobimetinib in *BRAF*-mutated melanoma. *N. Engl. J. Med*. 371:1867–1876. doi:10.1056/nejmoa1408868.

Lazaroff, J., and D. Bolotin. 2023. Targeted therapy and immunotherapy in melanoma. *Dermatol. Clin*. 41:65–77. doi:10.1016/j.det.2022.07.007.

Lee, L.M.J., E.A. Seftor, G. Bonde, R.A. Cornell, and M.J.C. Hendrix. 2005. The fate of human malignant melanoma cells transplanted into zebrafish embryos: Assessment of migration and cell division in the absence of tumor formation. *Dev. Dyn*. 233:1560–1570. doi:10.1002/dvdy.20471.

Li, Y., Z. Jia, S. Zhang, and X. He. 2021. Progress in gene-editing technology of zebrafish. *Biomolecules*. 11:1300. doi:10.3390/biom11091300.

Lister, J.A., C.P. Robertson, T. Lepage, S.L. Johnson, and D.W. Raible. 1999. *nacre* encodes a zebrafish microphthalmia-related protein that regulates neural-crest-derived pigment cell fate. *Development*. 126:3757–3767. doi:10.1242/dev.126.17.3757.

Long, G.V., C. Fung, A.M. Menzies, G.M. Pupo, M.S. Carlino, J. Hyman, H. Shahheydari, V. Tembe, J.F. Thompson, R.P. Saw, J. Howle, N.K. Hayward, P. Johansson, R.A. Scolyer, R.F. Kefford, and H. Rizos. 2014a. Increased MAPK reactivation in early resistance to dabrafenib/trametinib combination therapy of BRAF-mutant metastatic melanoma. *Nat. Commun*. 5:5694. doi:10.1038/ncomms6694.

Long, G.V., D. Stroyakovskiy, H. Gogas, E. Levchenko, F. De Braud, J. Larkin, C. Garbe, T. Jouary, A. Hauschild, J.J. Grob, V. Chiarion Sileni, C. Lebbe, M. Mandalà, M. Millward, A. Arance, I. Bondarenko, J.B.A.G. Haanen, J. Hansson, J. Utikal, V. Ferraresi, N. Kovalenko, P. Mohr, V. Probachai, D. Schadendorf, P. Nathan, C. Robert, A. Ribas, D.J. DeMarini, J.G. Irani, M. Casey, D. Ouellet, A.-M. Martin, N. Le, K. Patel, and K. Flaherty. 2014b.

Combined BRAF and MEK Inhibition versus BRAF Inhibition Alone in Melanoma. *N. Engl. J. Med*. 371:1877–1888. doi:10.1056/nejmoa1406037.

Long, G.V., D. Stroyakovskiy, H. Gogas, E. Levchenko, F. De Braud, J. Larkin, C. Garbe, T. Jouary, A. Hauschild, J.-J. Grob, V. Chiarion-Sileni, C. Lebbe, M. Mandalà, M. Millward, A. Arance, I. Bondarenko, J.B.A.G. Haanen, J. Hansson, J. Utikal, V. Ferraresi, N. Kovalenko, P. Mohr, V. Probachai, D. Schadendorf, P. Nathan, C. Robert, A. Ribas, D.J. DeMarini, J.G. Irani, S. Swann, J.J. Legos, F. Jin, B. Mookerjee, and K. Flaherty. 2015. Dabrafenib and trametinib versus dabrafenib and placebo for Val600 BRAF-mutant melanoma: a multicentre, double-blind, phase 3 randomised controlled trial. *Lancet*. 386:444–451. doi:10.1016/s0140-6736(15)60898-4.

Long, G.V., U. Trefzer, M.A. Davies, R.F. Kefford, P.A. Ascierto, P.B. Chapman, I. Puzanov, A. Hauschild, C. Robert, A. Algazi, L. Mortier, H. Tawbi, T. Wilhelm, L. Zimmer, J. Switzky, S. Swann, A.-M. Martin, M. Guckert, V. Goodman, M. Streit, J.M. Kirkwood, and D. Schadendorf. 2012. Dabrafenib in patients with Val600Glu or Val600Lys BRAF-mutant melanoma metastatic to the brain (BREAK-MB): a multicentre, open-label, phase 2 trial. *Lancet Oncol*. 13:1087–1095. doi:10.1016/s1470-2045(12)70431-x.

Lopes, J., C.M.P. Rodrigues, M.M. Gaspar, and C.P. Reis. 2022. Melanoma management: From epidemiology to treatment and latest advances. *Cancers*. 14:4652. doi:10.3390/cancers14194652.

Lorenzini, F., J. Marines, J. Le Friec, N. Do Khoa, M.A. Nieto, B. Sanchez-Laorden, M.C. Mione, L. Fontenille, and K. Kissa. 2025. Melanoma innervation, noradrenaline and cancer progression in zebrafish xenograft model. *Cell Death Discov.* 11:260. doi:10.1038/s41420-025-02523-8.

Lovly, C.M., K.B. Dahlman, L.E. Fohn, Z. Su, D. Dias-Santagata, D.J. Hicks, D. Hucks, E. Berry, C. Terry, M. Duke, Y. Su, T. Sobolik-Delmaire, A. Richmond, M.C. Kelley, C.L. Vnencak-Jones, A.J. Iafrate, J. Sosman, and W. Pao. 2012. Routine multiplex mutational profiling of melanomas enables enrollment in genotype-driven therapeutic trials. *PLoS One*. 7:e35309. doi:10.1371/journal.pone.0035309.

Lu, Y., and E.E. Patton. 2022. Long-term non-invasive drug treatments in adult zebrafish that lead to melanoma drug resistance. *Dis. Model. Mech*. 15:dmm049401. doi:10.1242/dmm.049401.

MacRae, C.A., and R.T. Peterson. 2023. Zebrafish as a mainstream model for in vivo systems pharmacology and toxicology. *Annu. Rev. Pharmacol. Toxicol.* 63:43–64. doi:10.1146/annurev-pharmtox-051421-105617.

Maresca, L., B. Stecca, and L. Carrassa. 2022. Novel therapeutic approaches with DNA damage response inhibitors for melanoma treatment. *Cells*. 11:1466. doi:10.3390/cells11091466.

Mendoza, M.C., E.E. Er, and J. Blenis. 2011. The Ras-ERK and PI3K-mTOR pathways: cross-talk and compensation. *Trends in Biochem. Sci*. 36:320–328. doi:10.1016/j.tibs.2011.03.006.

Miller, K.D., M. Fidler-Benaoudia, T.H. Keegan, H.S. Hipp, A. Jemal, and R.L. Siegel. 2020. Cancer statistics for adolescents and young adults, 2020. *CA Cancer J. Clinicians*. 70:443–459. doi:10.3322/caac.21637.

Mittapalli, R.K., S. Vaidhyanathan, A.Z. Dudek, and W.F. Elmquist. 2013. Mechanisms limiting distribution of the threonine-protein kinase B-RaF^{V600E} inhibitor dabrafenib to the brain: Implications for the treatment of melanoma brain metastases. *J. Pharmacol. Exp. Ther*. 344:655–664. doi:10.1124/jpet.112.201475.

Moore, J.C., Q. Tang, N.T. Yordán, F.E. Moore, E.G. Garcia, R. Lobbardi, A. Ramakrishnan, D.L. Marvin, A. Anselmo, R.I. Sadreyev, and D.M. Langenau. 2016. Single-cell imaging of normal and malignant cell engraftment into optically clear *prkdc*-null SCID zebrafish. *J. Exp. Med*. 213:2575–2589. doi:10.1084/jem.20160378.

Mouti, M.A., C. Dee, S.E. Coupland, and A.F.L. Hurlstone. 2016. Minimal contribution of ERK1/2-MAPK signalling towards the maintenance of oncogenic GNAQ^{Q209P}-driven uveal melanomas in zebrafish. *Oncotarget*. 7:39654–39670. doi:10.18632/oncotarget.9207.

Nasiadka, A., and M.D. Clark. 2012. Zebrafish breeding in the laboratory environment. *ILAR J*. 53:161–168. doi:10.1093/ilar.53.2.161.

Natarelli, N., S.J. Aleman, I.M. Mark, J.T. Tran, S. Kwak, E. Botto, S. Aflatooni, M.J. Diaz, and S.R. Lipner. 2024. A review of current and pipeline drugs for treatment of melanoma. *Pharmaceuticals*. 17:214. doi:10.3390/ph17020214.

Ng, M.F., J.L. Simmons, and G.M. Boyle. 2022. Heterogeneity in melanoma. *Cancers*. 14:3030. doi:10.3390/cancers14123030.

Nissan, M.H., C.A. Pratilas, A.M. Jones, R. Ramirez, H. Won, C. Liu, S. Tiwari, L. Kong, A.J. Hanrahan, Z. Yao, T. Merghoub, A. Ribas, P.B. Chapman, R. Yaeger, B.S. Taylor, N. Schultz, M.F. Berger, N. Rosen, and D.B. Solit. 2014. Loss of NF1 in cutaneous melanoma is associated with RAS activation and MEK dependence. *Cancer Res*. 74:2340–2350. doi:10.1158/0008-5472.can-13-2625.

Ouellet, D., E. Gibiansky, C. Leonowens, A. O'Hagan, P. Haney, J. Switzky, and V.L. Goodman. 2014. Population pharmacokinetics of dabrafenib, a BRAF inhibitor: Effect of dose, time, covariates, and relationship with its metabolites. *J. Clin. Pharmacol*. 54:696–706. doi:10.1002/jcph.263.

Patton, E.E., H.R. Widlund, J.L. Kutok, K.R. Kopani, J.F. Amatruda, R.D. Murphey, S. Berghmans, E.A. Mayhall, D. Traver, C.D.M. Fletcher, J.C. Aster, S.R. Granter, A.T. Look, C. Lee, D.E. Fisher, and L.I. Zon. 2005. BRAF mutations are sufficient to promote nevi formation and cooperate with p53 in the genesis of melanoma. *Curr. Biol*. 15:249–254. doi:10.1016/j.cub.2005.01.031.

Patton, E.E., L.I. Zon, and D.M. Langenau. 2021. Zebrafish disease models in drug discovery: from preclinical modelling to clinical trials. *Nat. Rev. Drug Discov*. 20:611–628. doi:10.1038/s41573-021-00210-8.

Piperno-Neumann, S., M.S. Carlino, V. Boni, D. Loirat, F.M. Speetjens, J.J. Park, E. Calvo, R.D. Carvajal, M. Nyakas, J. Gonzalez-Maffe, X. Zhu, M.D. Shirley, T. Ramkumar, A. Fessehatsion, H.E. Burks, P. Yerramilli-Rao, and E. Kapiteijn. 2023. A phase I trial of LXS196, a protein kinase C (PKC) inhibitor, for metastatic uveal melanoma. *Br. J. Cancer*. 128:1040–1051. doi:10.1038/s41416-022-02133-6.

Pollock, P.M., U.L. Harper, K.S. Hansen, L.M. Yudt, M. Stark, C.M. Robbins, T.Y. Moses, G. Hostetter, U. Wagner, J. Kakareka, G. Salem, T. Pohida, P. Heenan, P. Duray, O. Kallioniemi, N.K. Hayward, J.M. Trent, and P.S. Meltzer. 2003. High frequency of BRAF mutations in nevi. *Nat. Genet*. 33:19–20. doi:10.1038/ng1054.

Poynter, J.N., J.T. Elder, D.R. Fullen, R.P. Nair, M.S. Soengas, T.M. Johnson, B. Redman, N.E. Thomas, and S.B. Gruber. 2006. BRAF and NRAS mutations in melanoma and melanocytic nevi. *Melanoma Res*. 16:267–273. doi:10.1097/01.cmr.0000222600.73179.f3.

Precazzini, F., M. Pancher, P. Gatto, A. Tushe, V. Adami, V. Anelli, and M.C. Mione. 2020. Automated *in vivo* screen in zebrafish identifies Clotrimazole as targeting a metabolic vulnerability in a melanoma model. *Dev. Biol*. 457:215–225. doi:10.1016/j.ydbio.2019.04.005.

Puszkiel, A., G. Noé, A. Bellesoeur, N. Kramkimel, M.-N. Paludetto, A. Thomas-Schoemann, M. Vidal, F. Goldwasser, E. Chatelut, and B. Blanchet. 2019. Clinical pharmacokinetics and pharmacodynamics of dabrafenib. *Clin. Pharmacokinet*. 58:451–467. doi:10.1007/s40262-018-0703-0.

Qian, J., and Y. Liu. 2025. Recent advances in adoptive cell therapy for cancer immunotherapy. *Front. Immunol.* 16:1665488. doi:10.3389/fimmu.2025.1665488.

Quiñonez-Silvero, C., K. Hübner, and W. Herzog. 2020. Development of the brain vasculature and the blood-brain barrier in zebrafish. *Dev. Biol*. 457:181–190. doi:10.1016/j.ydbio.2019.03.005.

Rabbie, R., P. Ferguson, C. Molina-Aguilar, D.J. Adams, and C.D. Robles-Espinoza. 2019. Melanoma subtypes: genomic profiles, prognostic molecular markers and therapeutic possibilities. *J. Pathol*. 247:539–551. doi:10.1002/path.5213.

Ram, T., A.K. Singh, A. Kumar, H. Singh, P. Pathak, M. Grishina, H. Khalilullah, M. Jaremko, A.-H. Emwas, A. Verma, and P. Kumar. 2023. MEK inhibitors in cancer treatment: structural insights, regulation, recent advances and future perspectives. *RSC Med. Chem.* 14:1837–1857. doi:10.1039/d3md00145h.

Robert, C., J.J. Grob, D. Stroyakovskiy, B. Karaszewska, A. Hauschild, E. Levchenko, V. Chiarion Sileni, J. Schachter, C. Garbe, I. Bondarenko, H. Gogas, M. Mandalá, J.B.A.G. Haanen, C. Lebbé, A. Mackiewicz, P. Rutkowski, P.D. Nathan, A. Ribas, M.A. Davies, K.T. Flaherty, P. Burgess, M. Tan, E. Gasal, M. Voi, D. Schadendorf, and G.V. Long. 2019. Five-year outcomes with dabrafenib plus trametinib in metastatic melanoma. *N. Engl. J. Med*. 381:626–636. doi:10.1056/nejmoa1904059.

Santamaria-Barria, J.A., and J.M.V. Mammen. 2022. Surgical management of melanoma: Advances and updates. *Curr. Oncol. Rep*. 24:1425–1432. doi:10.1007/s11912-022-01289-x.

Santoriello, C., E. Gennaro, V. Anelli, M. Distel, A. Kelly, R.W. Köster, A. Hurlstone, and M. Mione. 2010. Kita driven expression of oncogenic HRAS leads to early onset and highly penetrant melanoma in zebrafish. *PLoS One*. 5:e15170. doi:10.1371/journal.pone.0015170.

Sarnaik, A.A., O. Hamid, N.I. Khushalani, K.D. Lewis, T. Medina, H.M. Kluger, S.S. Thomas, E. Domingo-Musibay, A.C. Pavlick, E.D. Whitman, S. Martin-Algarra, P. Corrie, B.D. Curti, J. Oláh, J. Lutzky, J.S. Weber, J.M.G. Larkin, W. Shi, T. Takamura, M. Jagasia, H. Qin, X. Wu, C. Chartier, F. Graf Finckenstein, M. Fardis, J.M. Kirkwood, and J.A. Chesney. 2021. Lifileucel, a tumor-infiltrating lymphocyte therapy, in metastatic melanoma. *J. Clin. Oncol*. 39:2656–2666. doi:10.1200/jco.21.00612.

Shain, A.H., and B.C. Bastian. 2016. From melanocytes to melanomas. *Nat. Rev. Cancer*. 16:345–358. doi:10.1038/nrc.2016.37.

Shi, W. 2015. Role for radiation therapy in melanoma. *Surg. Oncol. Clin. N. Am*. 24:323–335. doi:10.1016/j.soc.2014.12.009.

Siegel, R.L., K.D. Miller, N.S. Wagle, and A. Jemal. 2023. Cancer statistics, 2023. *CA Cancer J. Clin*. 73:17–48. doi:10.3322/caac.21763.

Singh, A.K., A. Kumar, S. Thareja, and P. Kumar. 2023. Current insights into the role of BRAF inhibitors in treatment of melanoma. *Anticancer Agents Med. Chem.* 23:278–297. doi:10.2174/1871520622666220624164152.

Sobhani, N., D.R. Tardiel-Cyril, A. Davtyan, D. Generali, R. Roudi, and Y. Li. 2021. CTLA-4 in regulatory T cells for cancer immunotherapy. *Cancers*. 13:1440. doi:10.3390/cancers13061440.

Spain, L., M. Julve, and J. Larkin. 2016. Combination dabrafenib and trametinib in the management of advanced melanoma with BRAFV600 mutations. *Expert Opin. Pharmacother*. 17:1031–1038. doi:10.1517/14656566.2016.1168805.

Sugino, Y., X. Bao, T. Kageyama, S. Sekito, S. Miyachi, T. Sasaki, T. Tanaka, and T. Inoue. 2025. Narrative review of patient cancer tissue–derived zebrafish xenograft models for evaluating drug sensitivity as an avatar model for clinical application. *Cancer Med*. 14:e70942. doi:10.1002/cam4.70942.

Tang, Q., N.S. Abdelfattah, J.S. Blackburn, J.C. Moore, S.A. Martinez, F.E. Moore, R. Lobbardi, I.M. Tenente, M.S. Ignatius, J.N. Berman, R.S. Liwski, Y. Houvras, and D.M. Langenau. 2014. Optimized cell transplantation using adult *rag2* mutant zebrafish. *Nat. Methods*. 11:821–824. doi:10.1038/nmeth.3031.

Tangella, L.P., M.E. Clark, and E.S. Gray. 2021. Resistance mechanisms to targeted therapy in BRAF-mutant melanoma - A mini review. *Biochim. Biophys. Acta Gen. Subj.* 1865:129736. doi:10.1016/j.bbagen.2020.129736.

Teame, T., Z. Zhang, C. Ran, H. Zhang, Y. Yang, Q. Ding, M. Xie, C. Gao, Y. Ye, M. Duan, and Z. Zhou. 2019. The use of zebrafish (*Danio rerio*) as biomedical models. *Anim. Front*. 9:68–77. doi:10.1093/af/vfz020.

Thomas, A.C., Z. Zeng, J.-B. Rivière, R. O'Shaughnessy, L. Al-Olabi, J. St.-Onge, D.J. Atherton, H. Aubert, L. Bagazgoitia, S. Barbarot, E. Bourrat, C. Chiaverini, W.K. Chong, Y. Duffourd, M. Glover, L. Groesser, S. Hadj-Rabia, H. Hamm, R. Happle, I. Mushtaq, J.-P. Lacour, R. Waelchli, M. Wobser, P. Vabres, E.E. Patton, and V.A. Kinsler. 2016. Mosaic Activating Mutations in GNA11 and GNAQ Are Associated with Phakomatosis Pigmentovascularis and Extensive Dermal Melanocytosis. *J. Invest. Dermatol*. 136:770–778. doi:10.1016/j.jid.2015.11.027.

Topczewska, J.M., L.-M. Postovit, N.V. Margaryan, A. Sam, A.R. Hess, W.W. Wheaton, B.J. Nickoloff, J. Topczewski, and M.J.C. Hendrix. 2006. Embryonic and tumorigenic pathways converge via Nodal signaling: role in melanoma aggressiveness. *Nat. Med*. 12:925–932. doi:10.1038/nm1448.

Traver, D., A. Winzeler, H.M. Stern, E.A. Mayhall, D.M. Langenau, J.L. Kutok, A.T. Look, and L.I. Zon. 2004. Effects of lethal irradiation in zebrafish and rescue by hematopoietic cell transplantation. *Blood*. 104:1298–1305. doi:10.1182/blood-2004-01-0100.

U.S. Food & Drug Administration. 2013. Tafinlar FDA label. https://www.accessdata.fda.gov/drugsatfda_docs/label/2018/202806s010lbl.pdf (accessed September 9, 2025).

Vaienti, S., P. Calzari, and G. Nazzaro. 2023. Topical treatment of melanoma in situ, lentigo maligna, and lentigo maligna melanoma with imiquimod cream: A systematic review of the literature. *Dermatol. Ther.* 13:2187–2215. doi:10.1007/s13555-023-00993-1.

Van Raamsdonk, C.D., V. Bezrookove, G. Green, J. Bauer, L. Gaugler, J.M. O'Brien, E.M. Simpson, G.S. Barsh, and B.C. Bastian. 2009. Frequent somatic mutations of *GNAQ* in uveal melanoma and blue naevi. *Nature*. 457:599–602. doi:10.1038/nature07586.

Van Raamsdonk, C.D., K.G. Griewank, M.B. Crosby, M.C. Garrido, S. Vemula, T. Wiesner, A.C. Obenauf, W. Wackernagel, G. Green, N. Bouvier, M.M. Sozen, G. Baimukanova, R. Roy, A. Heguy, I. Dolgalev, R. Khanin, K. Busam, M.R. Speicher, J. O'Brien, and B.C. Bastian. 2010. Mutations in GNA11 in Uveal Melanoma. *N. Engl. J. Med*. 363:2191–2199. doi:10.1056/nejmoa1000584.

Van Rooijen, E., M. Fazio, and L.I. Zon. 2017. From fish bowl to bedside: The power of zebrafish to unravel melanoma pathogenesis and discover new therapeutics. *Pigment Cell Melanoma Res*. 30:402–412. doi:10.1111/pcmr.12592.

Wang, B., W. Zhang, G. Zhang, L. Kwong, H. Lu, J. Tan, N. Sadek, M. Xiao, J. Zhang, M. Labrie, S. Randell, A. Beroard, E. Sugarman, V.W. Rebecca, Z. Wei, Y. Lu, G.B. Mills, J. Field, J. Villanueva, X. Xu, M. Herlyn, and W. Guo. 2021. Targeting mTOR signaling overcomes acquired resistance to combined BRAF and MEK inhibition in *BRAF*-mutant melanoma. *Oncogene*. 40:5590–5599. doi:10.1038/s41388-021-01911-5.

Wang, M., X. Gao, and L. Zhang. 2025a. Recent global patterns in skin cancer incidence, mortality, and prevalence. *Chin. Med. J.* 138:185–192. doi:10.1097/cm9.0000000000003416.

Wang, X., S. Ma, S. Zhu, L. Zhu, and W. Guo. 2025b. Advances in immunotherapy and targeted therapy of malignant melanoma. *Biomedicines*. 13:225. doi:10.3390/biomedicines13010225.

White, R.M., J. Cech, S. Ratanasirintrawoot, C.Y. Lin, P.B. Rahl, C.J. Burke, E. Langdon, M.L. Tomlinson, J. Mosher, C. Kaufman, F. Chen, H.K. Long, M. Kramer, S. Datta, D. Neuberg, S. Granter, R.A. Young, S. Morrison, G.N. Wheeler, and L.I. Zon. 2011. DHODH modulates transcriptional elongation in the neural crest and melanoma. *Nature*. 471:518–522. doi:10.1038/nature09882.

White, R.M., A. Sessa, C. Burke, T. Bowman, J. LeBlanc, C. Ceol, C. Bourque, M. Dovey, W. Goessling, C.E. Burns, and L.I. Zon. 2008. Transparent adult zebrafish as a tool for in vivo transplantation analysis. *Cell Stem Cell*. 2:183–189. doi:10.1016/j.stem.2007.11.002.

Yaeger, R., M.A. McKean, R. Haq, J.T. Beck, M.H. Taylor, J.E. Cohen, D.W. Bowles, S.M. Gadgeel, C. Mihalcioiu, K.P. Papadopoulos, E.L. Diamond, K.B. Sturtz, G. Feng, S.K. Drescher, M.B. Reddy, B. Sengupta, A.K. Maity, S.A. Brown, A. Singh, E.N. Brown, B.R. Baer, J. Wong, T.-C. Mou, W.-I. Wu, D.R. Kahn, S. Gadal, N. Rosen, J.J. Gaudino, P.A. Lee, D.P. Hartley, and S.M. Rothenberg. 2024. A next-generation BRAF inhibitor overcomes resistance to BRAF inhibition in patients with *BRAF*-mutant cancers using pharmacokinetics-informed dose escalation. *Cancer Discov*. 14:1599–1611. doi:10.1158/2159-8290.cd-24-0024.

Yan, C., D.C. Brunson, Q. Tang, D. Do, N.A. Iftimia, J.C. Moore, M.N. Hayes, A.M. Welker, E.G. Garcia, T.D. Dubash, X. Hong, B.J. Drapkin, D.T. Myers, S. Phat, A. Volorio, D.L. Marvin, M. Ligorio, L. Dershowitz, K.M. McCarthy, M.N. Karabacak, J.A. Fletcher, D.C. Sgroi, J.A. Iafrate, S. Maheswaran, N.J. Dyson, D.A. Haber, J.F. Rawls, and D.M. Langenau. 2019. Visualizing engrafted human cancer and therapy responses in immunodeficient zebrafish. *Cell*. 177:1903-1914.e14. doi:10.1016/j.cell.2019.04.004.

Yen, J., R.M. White, D.C. Wedge, P. Van Loo, J. De Ridder, A. Capper, J. Richardson, D. Jones, K. Raine, I.R. Watson, C.-J. Wu, J. Cheng, I. Martincorena, S. Nik-Zainal, L. Mudie, Y. Moreau, J. Marshall, M. Ramakrishna, P. Tarpey, A. Shlien, I. Whitmore, S. Gamble, C. Latimer, E. Langdon, C. Kaufman, M. Dovey, A. Taylor, A. Menzies, S. McLaren, S. O'Meara, A. Butler, J. Teague, J. Lister, L. Chin, P. Campbell, D.J. Adams, L.I. Zon, E.E. Patton, D.L. Stemple, and P.A. Futreal. 2013. The genetic heterogeneity and mutational burden of engineered melanomas in zebrafish models. *Genome Biol*. 14:R113. doi:10.1186/gb-2013-14-10-r113.

Yin, J., G. Forn-Cuní, A.M. Surendran, B. Lopes-Bastos, N. Pouliopoulou, M.J. Jager, S.E. Le Dévédec, Q. Chen, and B.E. Snaar-Jagalska. 2024. Lactate secreted by glycolytic conjunctival melanoma cells attracts and polarizes macrophages to drive angiogenesis in zebrafish xenografts. *Angiogenesis*. 27:703–717. doi:10.1007/s10456-024-09930-y.

Yin, J., G. Zhao, H. Kalirai, S.E. Coupland, A.G. Jochemsen, G. Forn-Cuní, A.P.A. Wierenga, M.J. Jager, B.E. Snaar-Jagalska, and A. Groenewoud. 2023. Zebrafish patient-derived xenograft model as a preclinical platform for uveal melanoma drug discovery. *Pharmaceuticals*. 16:598. doi:10.3390/ph16040598.

Zhang, Y., D. Song, X. Han, H. Liu, Y. Wang, X. Wang, and C. Dou. 2024. Unlocking the potential of melanotransferrin (CD228): implications for targeted drug development and novel therapeutic avenues. *Expert Opin. Ther. Targets*. 28:1117–1129. doi:10.1080/14728222.2024.2441705.

Zhang, Y., and X. Wang. 2020. Targeting the Wnt/β-catenin signaling pathway in cancer. *J. Hematol. Oncol*. 13:165. doi:10.1186/s13045-020-00990-3.

Zhong, J., W. Yan, C. Wang, W. Liu, X. Lin, Z. Zou, W. Sun, and Y. Chen. 2022. BRAF inhibitor resistance in melanoma: Mechanisms and alternative therapeutic strategies. *Curr. Treat. Options Oncol.* 23:1503–1521. doi:10.1007/s11864-022-01006-7.

8 Supplementary material

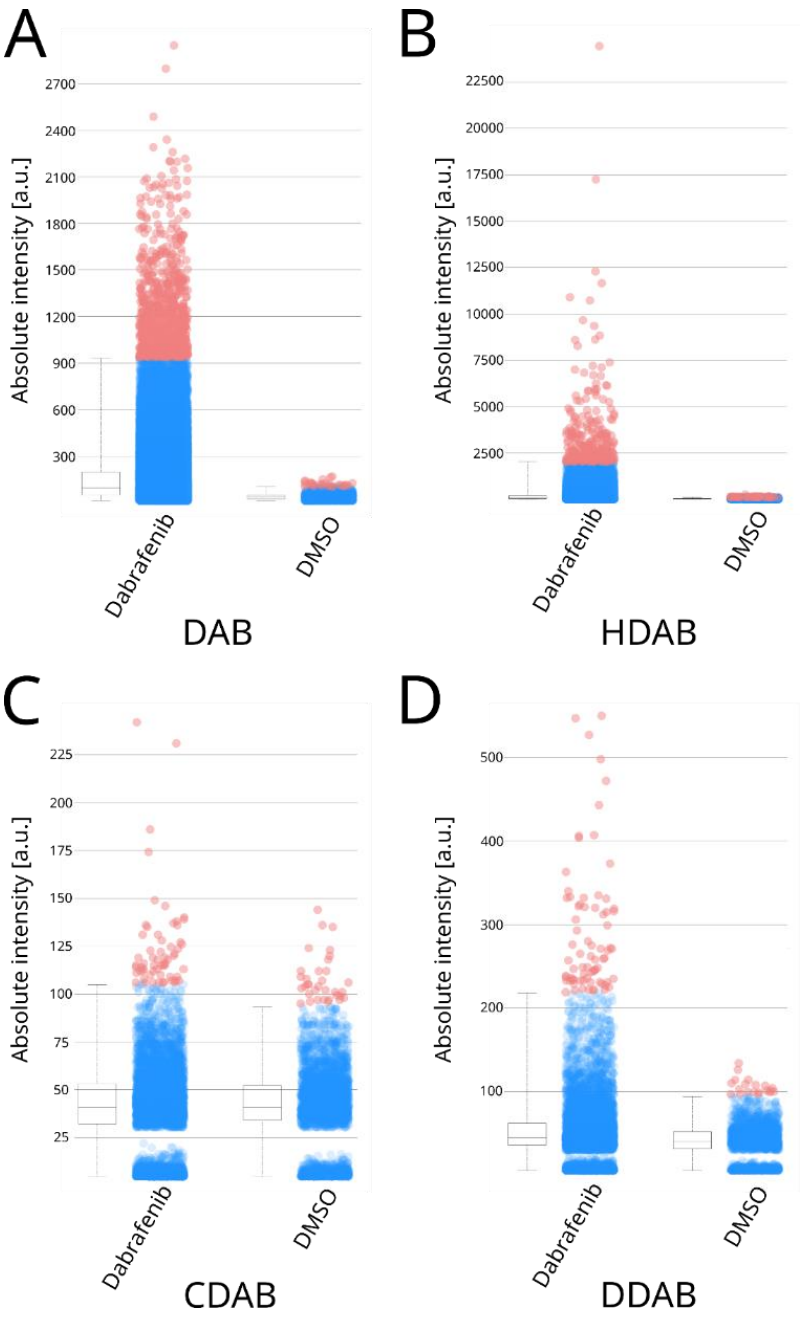

Supplementary figure 1. Quantification of mass spectrometry imaging. The pixel intensity of selected ion was observed using MALDI-MSI of dabrafenib and its most important metabolites in dabrafenib-treated (n=6) and control (n=2) zebrafish. A. Dabrafenib. B. Hydroxy-dabrafenib. C. Carboxy-dabrafenib. D. Desmethyl-dabrafenib.

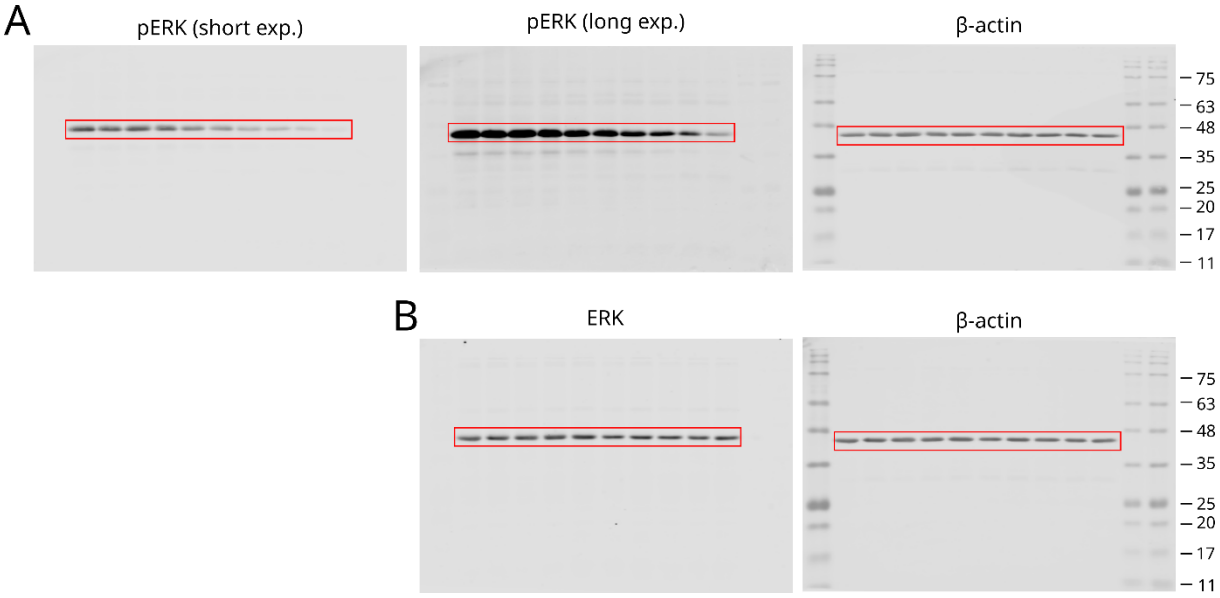

Supplementary figure 2. Uncropped Western blots for Fig. 11A. Membranes were probed with phospho-ERK (pERK) (A) or ERK (B) (700 nm channel) and reprobed with loading control β-actin (800 nm channel). Molecular weight markers are indicated, and the regions corresponding to each figure subpanel are highlighted in red.

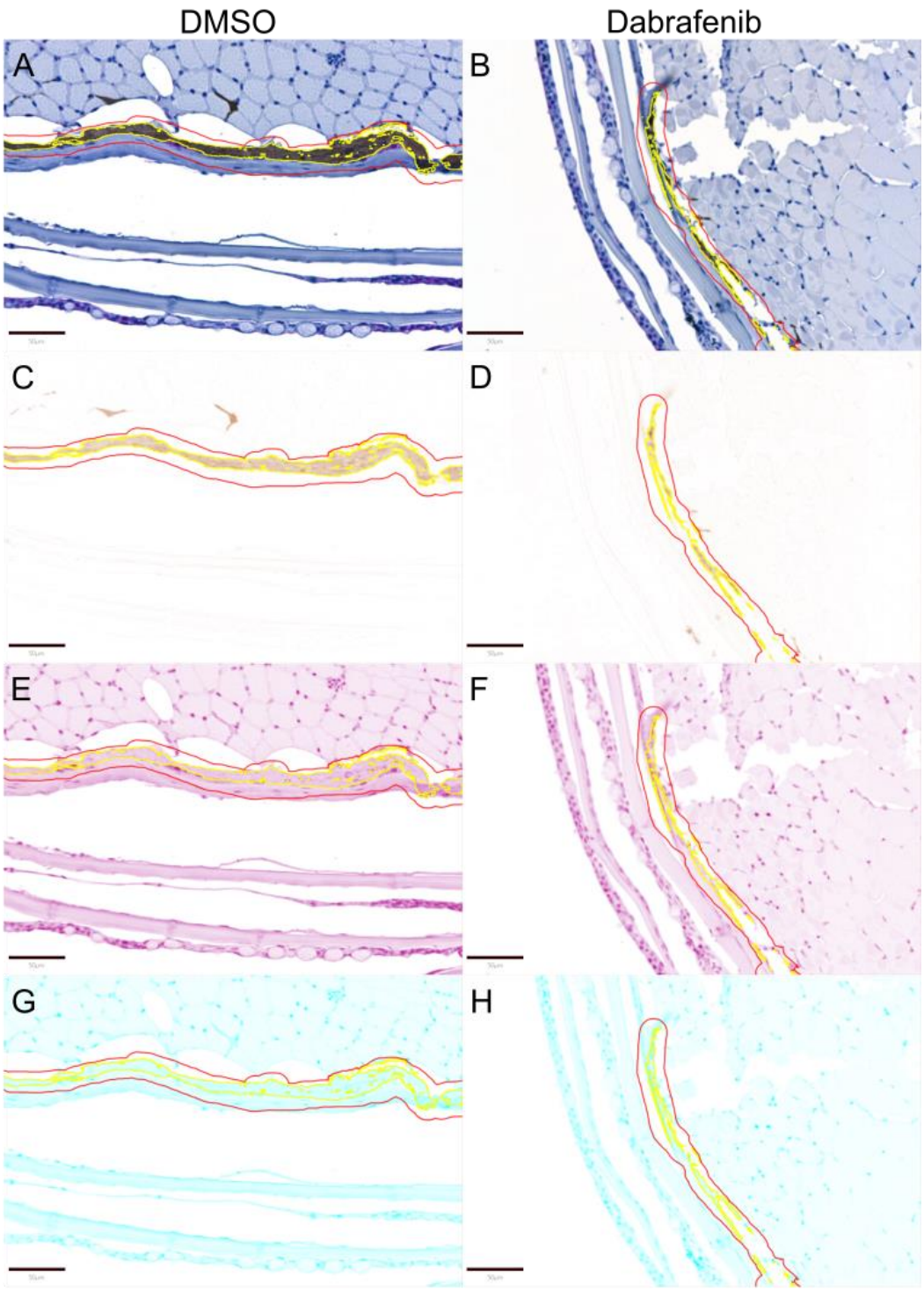

Supplementary figure 3. Colour deconvolution analysis of phospho-ERK immunohistochemistry staining of histological sections. Red line indicates manually annotated tumour region, and yellow line outlines the area measured and identified through threshold-based segmentation. Stain vectors were separated using colour deconvolution to separate channels. A. Brightfield image of control fish. B. Brightfield image of dabrafenib-treated fish. C. Brown channel showing melanoma of control fish. D. Brown channel showing melanoma of dabrafenib-treated fish. E. Pink channel showing DAB staining of phospho-ERK in control fish. F. Pink channel showing DAB staining of phospho-ERK in dabrafenib-treated fish. G. Residual channel of control fish. H. Residual channel of dabrafenib-treated fish. Scale bar = 50μm.